Supporting Information

for

Pre-Equilibrium Reactions Involving Pendent Relays Improve CO_2 Reduction Mediated by Molecular Cr-based Electrocatalysts

Megan E. Moberg, Amelia G. Reid, Diane A. Dickie, and Charles W. Machan*

* - machan@virginia.edu; ORCID 0000-0002-5182-1138

MEM ORCID 0000-0003-2083-9877; AGR ORCID 0000-0002-2868-4091; DAD ORCID 0000-0003-0939-3309

Department of Chemistry, University of Virginia, PO Box 400319, Charlottesville, VA 22904-4319

Table of Contents

Materials and Methods

General

All chemicals and solvents (ACS or HPLC grade) were commercially available and used as received unless otherwise indicated. For all air-sensitive reactions and electrochemical experiments, HPLC-grade solvents were obtained as anhydrous and air-free from a PPT Glass Contour Solvent Purification System. Gas cylinders were obtained from Praxair (Ar as 5.0; CO_2 as 4.0) and passed through activated molecular sieves prior to use. Gas mixing for variable concentration experiments was accomplished using a gas proportioning rotameter from Omega Engineering. UV-vis absorbance spectra were obtained on a Cary 60 from Agilent. An Anton-Parr Multiwave Pro SOLV, NXF-8 microwave reactor was used for microwave syntheses.

Electrochemistry

All electroanalytical experiments were performed using a Metrohm Autolab PGSTAT302N or a BioLogic SP-50 potentiostat. Glassy carbon disc working electrodes (⌀ = 3 mm) and non-aqueous silver/silver chloride pseudoreference electrodes behind PTFE tips were obtained from CH Instruments. The pseudoreference electrodes were obtained by depositing chloride on bare silver wire in 10% HCl at oxidizing potentials and stored in a 0.1 M tetrabutylammonium hexafluorophosphate/*N*,*N*-dimethylformamide ($TBAPF_6$/DMF) solution in the dark prior to use. The counter electrode was a glassy carbon rod (⌀ = 3 mm). All CV experiments were performed in a modified scintillation vial (20 mL volume) as a single-chamber cell with a cap modified with ports for all electrodes and a sparging needle. $TBAPF_6$ was purified by recrystallization from ethanol and dried in a vacuum oven before being stored in a vacuum desiccator. All data were referenced to an internal ferrocene standard (ferricenium/ferrocene (Fc^+/Fc) reduction potential under stated conditions) unless otherwise specified. Ferrocene was purified by sublimation prior to use. All voltammograms were corrected for internal resistance.

Controlled Potential Electrolysis (CPE)

CPE experiments were performed in a glass Pine Research Instrumentation H-cell with two compartments separated by a glass frit. A 75 mL stock solution of DMF with 0.1 M $TBAPF_6$ was prepared for each bulk electrolysis experiment unless otherwise noted. Approximately 26 mL of the stock solution was added to each half of the H-cell. One side of the H-cell contained the catalyst, any additional substrate, such as the proton source, and a glassy carbon rod working electrode. The other side of the H-cell contained approximately 0.075 M ferrocene as a sacrificial reductant along with a graphite rod counter electrode and a Ag/AgCl pseudoreference electrode. The electrolysis experiment was referenced by taking a CV of the side of the H-cell that contained the ferrocene solution. The H-cell was sealed with two septa that were connected by a piece of PTFE tubing which aided to maintain equal pressure between each half of the cell during the electrolysis. Before starting the electrolysis experiment, both sides of the H-cell were sparged with the indicated gas for 20 minutes and the sealed cell was allowed to equilibrate for 1 hour. The resistance between the two halves of the H-cell was measured using the i-interrupt procedure available in the NOVA software provided by Metrohm and corrected for this value.

CPE Product Analysis

During CPE experiments, 100 or 250 μL GC injections of the headspace were periodically taken for the detection and quantification of any gaseous products produced. After each CPE experiment, the total volume of solution was measured. The total volume of the sealed H-cell was also measured to account for the total headspace volume for accurate quantification of gaseous products. A calibration curve for CO and H_2 was used to quantify gaseous products produced during electrolysis experiments in the same manner as we previously reported.[1]

Analysis of gas phase products was done by sampling electrolysis headspace through syringe injections into an Agilent 7890B GC equipped with a specialty gas split column 5 Å mol sieve/Porabond Q column (15 m length; 0.320 mm diameter; 25.0 μm film) and thermal conductivity detector with He as a carrier gas. A calibration curve for CO and H_2 was made in the H-cell with an experimental setup containing identical volumes of DMF in 0.1 M $TBAPF_6$ to those used during electrolysis. Known volumes of CO and H_2 were injected into the cell with stirring and 250 μL injections of the headspace were taken for GC injections after equilibration. The limit of detection (LOD) and limit of quantitation (LOQ) for CO and H_2 in the GC were determined from seven consecutive injections at the lowest observable concentrations of each gaseous product respectively. For CO, the LOD was determined to be 5.77 x 10^{-7} moles and the LOQ was determined to be 1.92 x 10^{-6} moles. For H_2, the LOD was determined to be 4.55 x 10^{-6} moles and the LOQ was determined to be 1.52 x 10^{-5} moles.

Calculation of Overpotential for CO_2 Reduction (Adapted)

The calculation of overpotential for all catalysts was performed according to reported methods.[2] The following equation was used for the determination of the reaction standard potential in V with respect to the Fc^+/Fc couple:

$$E_{CO2/CO} = -0.73\,V - 0.059(pK_a) \qquad \textbf{Eq (1)}$$

The pK_a and corresponding $E_{CO2/CO}$ for PhOH[3] and $TEAHPF_6$[4] are:

	PhOH	**$TEAHPF_6$**
pK_a(DMF)	18.8	9.25
$E_{CO2/CO}$ (V vs. Fc^+/Fc)	–1.84	–1.28

Note that the scaled pK_a values for TFE place the system at an underpotential (counterthermodynamic conditions) by method described below. This suggests limitations either with the computational method used to assess its pK_a,[5-7] or significant solvation and homoconjugation contributions (see below).

The $E_{cat/2}$ for protic CO_2 reduction is determined experimentally for each catalyst with 1.0 mM catalyst 0.1 M proton source. The overpotential is then determined according to:

$$\eta = \left|E_{cat/2} - E_{CO2/CO}\right| \qquad \textbf{Eq (2)}$$

Catalyst	Proton Source	$E_{cat/2}$ V *vs.* Fc^+/Fc	η V
Cr(^{tbu}dhbpy)Cl(H_2O)	PhOH	–1.95	0.11
	$TEAHPF_6$	N/A*	—
Cr($^{p\text{-}tbu}$dhbpy)Cl(H_2O)	PhOH	–1.95	0.09
	$TEAHPF_6$	N/A*	0.70
Cr(^{nPr}dhbpy)Cl(H_2O)	PhOH	–1.94	0.06
	$TEAHPF_6$	–1.89	0.66

* - significant heterogeneous current response is observed

This assumes no contribution from homoconjugation of the acid. We note that the homoconjugation constant (HA_2^-) for PhOH in DMF has been reported as $\log(K_{HA_2^-}) = 3.8$[8]; no homoconjugation constant is reported for TFE; and TEAH has a homoconjugation constant of approximately 0.[9] Therefore, we emphasize that the described overpotential calculated above for PhOH is the lower-limit approximation, as homoconjugation is expected to alter the effective overpotential. Although similar conditions are not expected for $TEAHPF_6$, as pointed out above there are additional issues with the reliable estimation of overpotential with TFE. The overpotential equation can be modified to account for homoconjugation:

$$E_{CO2/CO} = -0.73\,V - 0.059(pK_a) - \frac{-2.303RT}{nF}\log\,(mK_{HA_2^-}) \qquad \textbf{Eq (3)}$$

Where n = number of electrons (2) and m = number of proton transfers (2). The modified equation provides $E^0_{CO2/CO} = -1.72$ V and the following η values:

Cr(^{tbu}dhbpy)Cl(H_2O) $\eta = 0.23$ V
Cr($^{p\text{-}tbu}$dhbpy)Cl(H_2O) $\eta = 0.21$ V
Cr(^{nPr}dhbpy)Cl(H_2O) $\eta = 0.18$ V

This value does not account for the possible thermodynamic contributions of the water coordinated to the pre-catalyst, the equimolar quantities of water produced for each equivalent of CO generated, or any adventitious H_2O present in the CO_2, solvent, or electrolyte. Under CO_2 saturation, any water present can form carbonic acid, pK_a(DMF) 7.37,[10] and generate new equilibria involving CO_2 and bicarbonate. The role of carbonic acid (and the general hydration of CO_2 in non-aqueous solvent systems) in altering the overall thermodynamics combined with the effects of homoconjugation has been assessed by Matsubara.[11] Considering the role of water, Matsubara obtained a standard potential for CO_2 reduction to CO of −1.70 V versus Fc^+/Fc for PhOH in *N,N*-DMF with 10 mM water present (see below). Note the same value is obtained considering 10 mM water only.

For 10 mM H_2O in DMF, where AH = PhOH:[11]

$$3CO_{2(g)} + H_2O_{(sol,x)} + 2e^- \rightleftharpoons CO_{(g)} + 2HCO_{3\,(sol)}^- \qquad E^0 = -1.70\,V\ vs.\,Fc^+/Fc$$
$$CO_{2(g)} + 2AH_{(sol)} + 2e^- \rightleftharpoons CO_{(g)} + 2A^-_{(sol)} + H_2O_{(sol,x)} \qquad E^0 = -1.96\,V\ vs.\,Fc^+/Fc$$
$$CO_{2(g)} + 4AH_{(sol)} + 2e^- \rightleftharpoons CO_{(g)} + 2HA_{2\,(sol)}^- + H_2O_{(sol,x)} \qquad E^0 = -1.70\,V\ vs.\,Fc^+/Fc$$

Determination of TOF from Preparative Electrolysis

The integrated expression of current for a homogeneous electrocatalytic response (considering an application of steady-state conditions to the substrate) has been solved previously:[12, 13]

$$\frac{i}{FA} = \frac{n_{cat}^{\sigma}[cat]\sqrt{(k_{obs}D_{cat})}}{1 + \exp\left[\frac{F}{RT}\left(E_{app} - E_{1/2}\right)\right]} \text{where}$$

$$\frac{i}{A} = J = CO\ specific\ current\ density$$

Substituting and rearranging the first expression to solve for k_{obs}

$$k_{obs} = \frac{J^2\left(1 + \exp\left[\frac{F}{RT}\left(E_{app} - E_{1/2}\right)\right]\right)^2}{F^2(n_{cat}^{\sigma}[cat])^2 D_{cat}}$$

with k_{obs} in hand, the TOF can be expressed for a given potential according to the following relationship

$$TOF = \frac{k_{obs}}{1 + \exp\left[\frac{F}{RT}\left(E_{app} - E_{1/2}\right)\right]}$$

Parameters for CPE experiments reported here not found in **Table 1**.

- $E_{1/2}$ catalyst:
  - −1.95 V vs Fc^+/Fc for Cr(^{tbu}dhbpy)Cl(H_2O)[3]
  - −1.95 V vs Fc^+/Fc for Cr($^{p\text{-}tbu}$dhbpy)Cl(H_2O) **1**
  - −1.95 V vs Fc^+/Fc for Cr(^{nPr}dhbpy)Cl(H_2O) **2**
- Temperature: 298.15 K
- $[CO_2]$: 2.3 x 10^{-4} mol cm^{-3}
- Diffusion coefficient:
  - 2.0 x 10^{-6} cm^2 s^{-1} for Cr(^{tbu}dhbpy)Cl(H_2O)[15]
  - 2.9 x 10^{-6} cm^2 s^{-1} for Cr($^{p\text{-}tbu}$dhbpy)Cl(H_2O) **1**
  - 1.7 x 10^{-6} cm^2 s^{-1} for Cr(^{nPr}dhbpy)Cl(H_2O) **2**
- Electrode area: 2.04 cm^2, 2.23 cm^2, 2.29 cm^2, or 3.28 cm^2

Calculation of Diffusion Coefficients

The calculation of the diffusion coefficients for Cr($^{p\text{-}tbu}$dhbpy)Cl(H_2O) **1** and Cr(^{nPr}dhbpy)Cl(H_2O) **2** catalysts was performed by reported methods.[16] Cyclic voltammetry (CV) experiments were done with a solution of 1.0 mM catalyst in 0.1 M $TBAPF_6$/DMF under Ar saturation conditions. The scan rate of these CVs was varied from 25 mV/s to 5000 mV/s (**Figure S5A** and **S26A**). The increase in current observed as the scan rate increases can be represented by the following equation where i_p is the peak current, n is the number of electrons, A is the area of the electrode, D is the diffusion coefficient, C is the concentration of analyte, and v is the scan rate:

$$i_p = (2.69 \times 10^5)n^{3/2}ACD^{1/2}v^{1/2}$$

By plotting the current density as a function of $v^{1/2}$ (**Figure S5B** and **S26B**), the slope can be used to find *D*.

$$D_{cat} = \frac{(\text{slope})^2}{n^3 C^2 (2.69 \times 10^5)^2}$$

Determination of k_1 for Cr(^{nPr}dhbpy)Cl(H_2O) (2) with under CO_2 Saturation

All k_1 determinations were based on a reported procedure.[17] Using the evolution of $E_{cat/2}$ with respect to acid concentration, in the framework of an *ECEC′* mechanism, the rate constant for the first proton transfer can be determined, k_1. Here C_A^0 is the concentration of added acid and k_1 relates to the protonation of the $[Cr–CO_2]^-$ adduct species *iii* (**Figure 1**, Main Text). From **Eq (4)**[12] we can substitute the TOF_{CPE} for $k_2 C_Z^0$, which is the rate-determining step, since CV waves remain S-shaped and the catalytic current is saturated across analyzed proton donor concentrations.

$$k_{obs} = TOF = k_{cat}[\text{substrate}] \qquad \textbf{Eq (4)}^{12}$$

$$E_{1/2} = E^0_{P/Q} + \frac{RT}{F} \ln\left(1 + \frac{\sqrt{k_1 C_A^0}}{\sqrt{k_2 C_Z^0}}\right) \qquad \textbf{Eq (5)}^{17}$$

Where *R*, *T*, and *F* are the gas constant, temperature (in K), and Faraday's constant, respectively, $E_{1/2}$ is the potential of the irreversible catalytic feature, $E^0_{P/Q}$ is the potential of the one-electron reversible electrochemical event in the absence of substrate. A temperature of 298.15 K was used for any analysis.

Determination of Acid Equilibrium Binding Constant (K_Q) under Ar Saturation

Using the evolution of the $E_{1/2}$ of the catalytically relevant potential with respect to acid concentration, the equilibrium binding constant, K_Q for the interaction between $TEAH^+$ and $[Cr(^{nPr}dhbpy)]^-$ can be determined.[18]

$$E = E^0 + \left(\frac{RT}{nF}\right) ln(1 + [TEAHPF_6]K_Q) \qquad \textbf{Eq (6)}$$

Where *R*, *T*, and *F* are the gas constant, temperature (in K), and Faraday's constant, respectively, *n* is the number of electrons involved in the redox event, *E* is the potential of the one-electron reversible electrochemical event in the presence of substrate, E^0 is the potential of the one-electron reversible electrochemical event in the absence of substrate. A temperature of 298.15 K was used for any analysis.

Single Crystal X-ray Diffraction

A single crystal of **[Cr($^{p\text{-}tbu}$dhbpy)Cl]$_2$·6DMF** or **[Cr($^{p\text{-}tbu}$dhbpy)Cl]$_2$·8DMF** was coated with Paratone oil and mounted on a MiTeGen MicroLoop. The X-ray intensity data were measured on a Bruker D8 Venture Photon III Kappa four-circle diffractometer system equipped with both an Incoatec IμS 3.0 micro-focus sealed X-ray tube (Cu Kα, λ = 1.54178 Å) and a HELIOS MX double bounce multilayer mirror monochromator, and an Incoatec I μ S 3.0 micro-focus sealed X-ray tube (Mo K α, λ = 0.71073 Å) and a HELIOS double bounce multilayer mirror monochromator. The

frames were integrated with the Bruker SAINT software package[19] using a narrow-frame algorithm. Data were corrected for absorption effects using the Multi-Scan method (SADABS).[20] Each structure was solved and refined using the Bruker SHELXTL Software APEX5[19] and OLEX2.[21] Non-hydrogen atoms were refined anisotropically. Hydrogen atoms were placed in geometrically calculated positions with U_{iso} = 1.2U_{equiv} of the parent atom (U_{iso} = 1.5U_{equiv} for methyl). The relative occupancy of the disordered solvent molecules was freely refined. A combination of constraints and restraints was used on most of the disordered atoms and bond lengths.

Table S1. Crystallographic details for [Cr(p-^{tbu}dhbpy)Cl]$_2$·6DMF and [Cr(p-^{tbu}dhbpy)Cl]$_2$·8DMF

	[Cr(p-^{tbu}dhbpy)Cl]$_2$·6DMF	**[Cr(p-^{tbu}dhbpy)Cl]$_2$·8DMF**
CCDC number	2330314	2330315
Formula	$C_{78}H_{102}Cl_2Cr_2N_{10}O_{10}$	$C_{84}H_{116}Cl_2Cr_2N_{12}O_{12}$
FW (g/mol)	1513.28	1660.78
Temp (K)	100(2)	100(2)
λ (Å)	1.54178	0.71073
Size (mm)	0.039 x 0.082 x 0.144	0.107 x 0.130 x 0.185
Crystal habit	orange plate	red block
Crystal system	triclinic	triclinic
Space group	P -1	P -1
a (Å)	11.4779(5)	10.2564(11)
b(Å)	12.8869(7)	12.7752(13)
c (Å)	14.3534(8)	18.0002(17)
α (°)	81.222(4)	76.384(3)
β (°)	87.557(4)	77.776(3)
γ (°)	67.474(3)	68.844(3)
Volume (Å^3)	1937.84(18)	2116.7(4)
Z	1	1
Density (g/cm^3)	1.297	1.303
μ (mm^{-1})	3.453	0.386
F(000)	801	882
θ range (°)	3.12 to 68.39	2.27 to 25.73
Index ranges	-13 ≤ h ≤ 13 -15 ≤ k ≤ 15 -17 ≤ l ≤ 17	-12 ≤ h ≤ 12 -15 ≤ k ≤ 15 -17 ≤ l ≤ 21
Reflns collected	37038	41199
Independent reflns	7082 [R_{int} = 0.1131]	8045 [R_{int} = 0.0690]
Data / restraints /parameters	7082 / 385 / 615	8045 / 5 / 555
GOF on F^2	1.054	1.073
R_1 (I>2σ(I))	0.0882	0.0844
wR_2 (all data)	0.2707	0.2563

Synthesis and Characterization

Synthesis of 6,6′-di(5-*tert*-butyl-2-hydroxybenzene)-2,2′-bipyridine, $^{p\text{-}tbu}$dhbpy(H)$_2$

The synthesis of $^{p\text{-}tbu}$dhbpy(H)$_2$ was carried out as previously reported.[22]

Synthesis of Cr($^{p\text{-}tbu}$dhbpy)Cl(H$_2$O) (1)

Metallation of $^{p\text{-}tbu}$dhbpy(H)$_2$ to generate Cr($^{p\text{-}tbu}$dhbpy)Cl(H$_2$O) (**1**) was achieved by stirring $^{p\text{-}tbu}$dhbpy(H)$_2$ (0.200 g, 0.442 mmol) and 1.05 equivalents of chromium (II) dichloride (0.0570 g, 0.464 mmol) in tetrahydrofuran (100 mL) at reflux conditions under an inert atmosphere for 24 hrs. After exposing the reaction to air, the solution was filtered to collect the reaction precipitate. The solid was sonicated in saturated ammonium chloride (200 mL), filtered and then sonicated in water (200 mL). Upon the second filtration the solid was washed with hot hexanes (200 mL). 56.3 % isolated yield (0.138 g). Elemental analysis for $C_{30}H_{32}ClCrN_2O_3$ calc'd: C 64.80, H 5.80, N 5.04; found: C 64.96, H 5.43, N 5.08.

Synthesis of 6,6′-di(3-methoxy-5-*n*-propyl-2-hydroxybenzene)-2,2′-bipyridine, ^{nPr}dhbpy(H)$_2$

The synthesis of ^{nPr}dhbpy(H)$_2$ was carried out as previously reported.[22]

Synthesis of Cr(^{nPr}dhbpy)Cl(H$_2$O) (2)

Metalation of ^{nPr}dhbpy(H)$_2$ with Cr(II) to generate Cr(^{nPr}dhbpy)Cl(H$_2$O) (**2**) was achieved by stirring ^{nPr}dhbpy(H)$_2$ (0.200 g, 0.413 mmol) and 1.05 equivalents of chromium(II) dichloride (0.0533 g, 0.433 mmol) in tetrahydrofuran (100 mL) at room temperature under an inert atmosphere for 24 hrs. After exposing the reaction to air, the solution was filtered to collect the reaction precipitate. The solid was sonicated in saturated ammonium chloride (200 mL), filtered and then sonicated in water (200 mL). Upon the second filtration the solid was washed with hot hexanes (200 mL). 86.0 % isolated yield (0.208 g). Elemental analysis for $C_{30}H_{32}ClCrN_2O_5$ calc'd C 60.35, H 5.57, N 4.69; found: C 60.74, H 5.87, N 4.49.

Evans' Method Characterization of 1

The spin state of the Cr($^{p\text{-}tbu}$dhbpy)Cl(H$_2$O) (**1**) catalyst was characterized as a Cr(III) species via Evans' Method.[23, 24] Three capillary inserts were made with a 50% v/v mixture of DMF and DMF-d_7. Each insert was flame sealed, and then placed in an NMR tube. Then 15.5 mg of **1** was dissolved in 17 mL of DMF. Approximately 0.6 mL of the solution of **1** was added to each of the three NMR tubes containing a flame sealed insert. ^{1}H NMR spectra with 128 scans were then taken using a 600 MHz Varian NMR Spectrometer. The results of this experiment, which was run in triplicate, can be seen in **Table S1**. The average μ_{eff} of **1** was 4.1±0.2.

Table S2. Evans' method results for Cr($^{p\text{-}tbu}$dhbpy)Cl(H$_2$O) (1) in DMF.[23, 24]

Trial	Chemical Shift (ppm)	Chemical Shift (Hz)	Total Magnetic Moment (emu mol^{-1})	Paramagnetic Moment (emu mol^{-1})	μ_{eff} (Bohr Magnetons)
1	0.05	30	7.28 x 10^{-3}	7.67 x 10^{-3}	4.28
2	0.04	24	5.82 x 10^{-3}	6.21 x 10^{-3}	3.85
3	0.05	30	7.28 x 10^{-3}	7.67 x 10^{-3}	4.28

Evans' Method Characterization of 2

The spin state of the Cr(^{nPr}dhbpy)Cl(H_2O) (**2**) catalyst was characterized as a Cr(III) species via Evans' Method.[23, 24] Three capillary inserts were made with a 50% v/v mixture of DMF and DMF-d_7. Each insert was flame sealed, and then placed in an NMR tube. Then 14.6 mg of **2** was dissolved in 9 mL of DMF. Approximately 0.6 mL of the solution of **2** was added to each of the three NMR tubes containing a flame sealed insert. ^{1}H NMR spectra with 128 scans were then taken using a 600 MHz Varian NMR Spectrometer. The results of this experiment, which was run in triplicate, can be seen in **Table S2**. The average μ_{eff} of **2** was 4.2±0.3.

Table S3. Evans' method results for Cr(^{nPr}dhbpy)Cl(H_2O) (2) in DMF.[23, 24]

Trial	Chemical Shift (ppm)	Chemical Shift (Hz)	Total Magnetic Moment (emu mol^{-1})	Paramagnetic Moment (emu mol^{-1})	μ_{eff} (Bohr Magnetons)
1	0.09	54	7.78 x 10^{-3}	8.17 x 10^{-3}	4.41
2	0.07	42	6.05 x 10^{-3}	6.44 x 10^{-3}	3.92
3	0.09	54	7.78 x 10^{-3}	8.17 x 10^{-3}	4.41

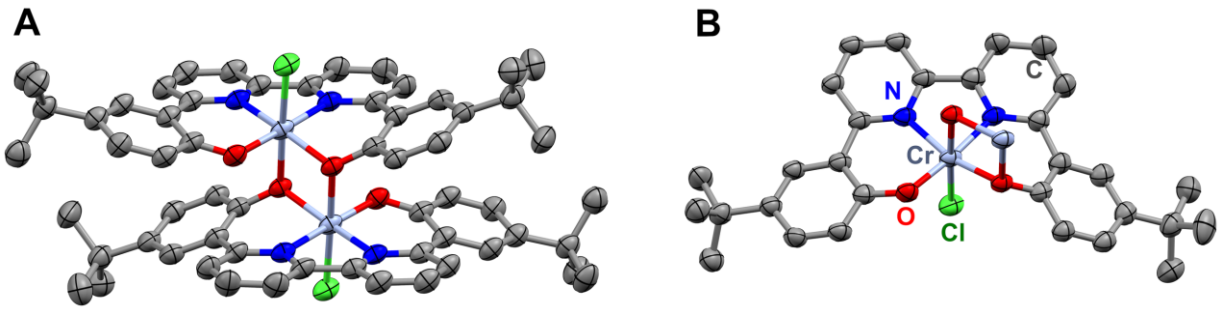

Figure S1. (**A**) The dimer structure of [Cr($^{p\text{-}tbu}$dhbpy)Cl]$_2$ obtained from single-crystal X-ray diffraction studies. Blue = N, red = O, gray = C; thermal ellipsoids at 50%; co-crystallized DMF solvent and H atoms omitted for clarity. CCDC 2330314. (**B**) The truncated structure showing connectivity at Cr for a single complex.

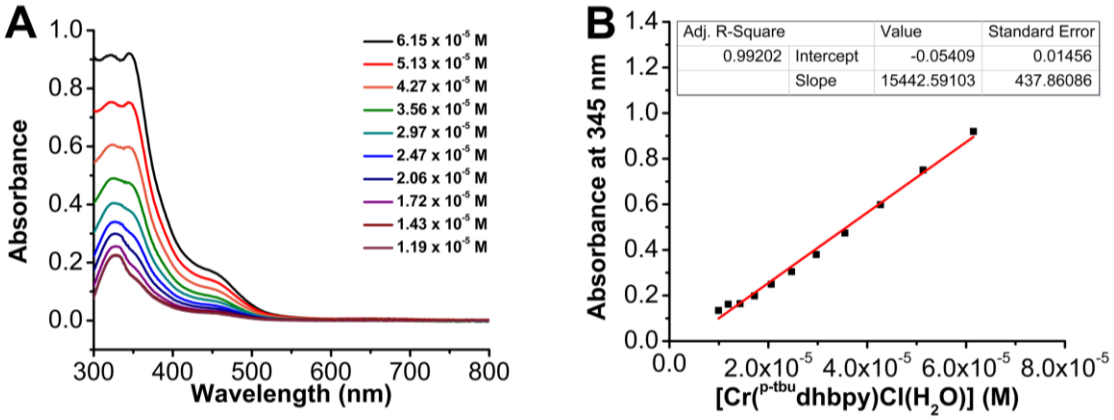

Figure S2. (**A**) UV-vis serial dilution absorbance data obtained from Cr($^{p\text{-tbu}}$dhbpy)Cl(H_2O) **1** in a DMF solution. Conditions: varying concentration; quartz cell with 1 cm pathlength. (**B**) Plot of absorbance versus concentration (M) for Cr($^{p\text{-tbu}}$dhbpy)Cl(H_2O) (**1**) in DMF at 345 nm (31100 M^{-1} cm^{-1}); R^2 = 0.992. All: λ_{max} = 320 nm (6430 M^{-1} cm^{-1}) and 448 nm (4900 M^{-1} cm^{-1}).

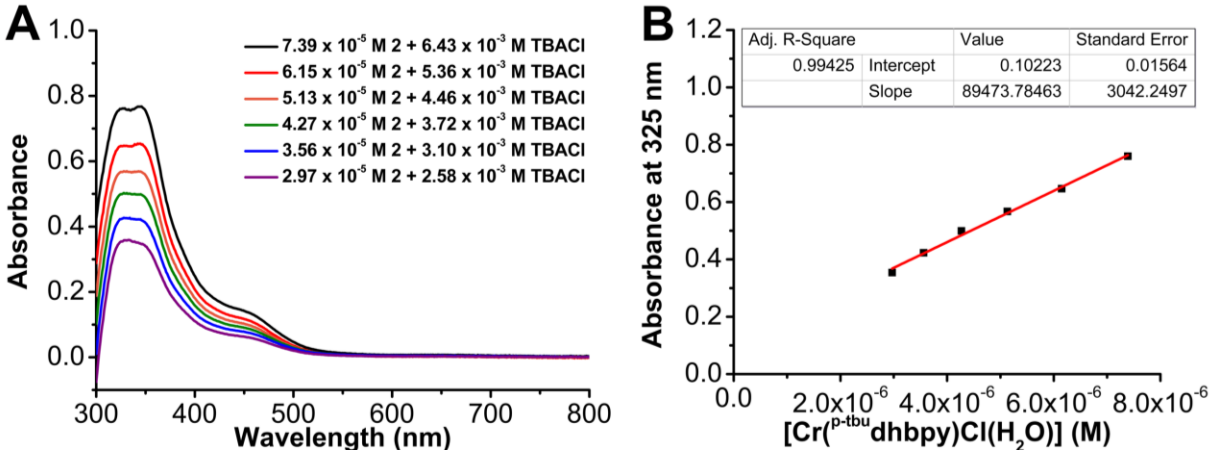

Figure S3. (**A**) UV-vis serial dilution absorbance data obtained from Cr($^{p\text{-tbu}}$dhbpy)Cl(H_2O) **1** and excess tetrabutylammonium chloride (TBACl) in a DMF solution. Conditions: varying concentration; quartz cell with 1 cm pathlength. (**B**) Plot of absorbance versus concentration (M) for Cr($^{p\text{-tbu}}$dhbpy)Cl(H_2O) (**1**) and excess TBACl in DMF at 325 nm (31100 M^{-1} cm^{-1}); R^2 = 0.992. All: λ_{max} = 345 nm (6430 M^{-1} cm^{-1}) and 457 nm (4900 M^{-1} cm^{-1}).

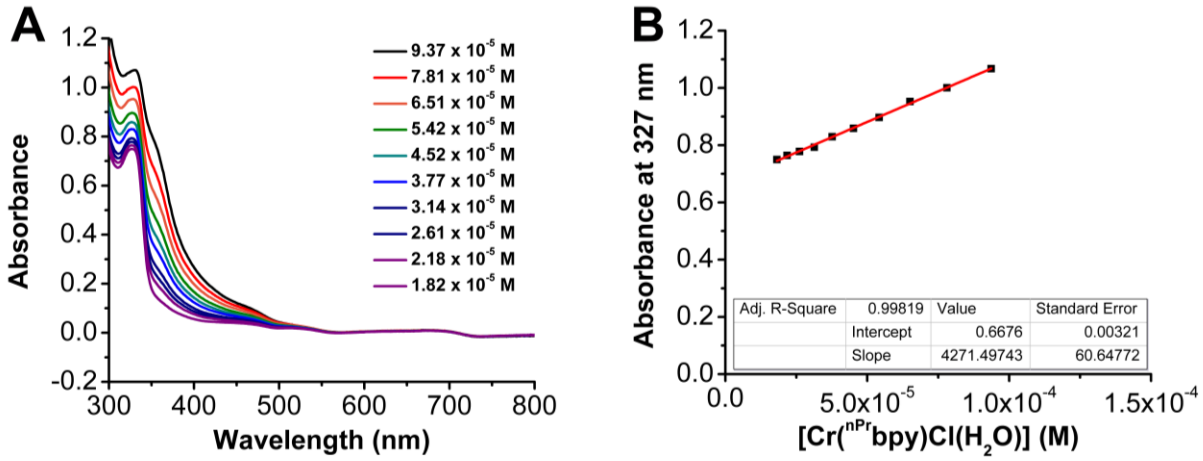

Figure S4. (**A**) UV-vis serial dilution absorbance data obtained from Cr(^{nPr}dhbpy)Cl(H_2O) **2** in a DMF solution. Conditions: varying concentration; quartz cell with 1 cm pathlength. (**B**) Plot of absorbance versus concentration (M) for Cr(^{nPr}dhbpy)Cl(H_2O) (**2**) in DMF at 327 nm (4270 M^{-1} cm^{-1}); R^2 = 0.999. All: λ_{max} = 360 nm (7500 M^{-1} cm^{-1}) and 455 nm (1000 M^{-1} cm^{-1}).

Electrochemistry of 1

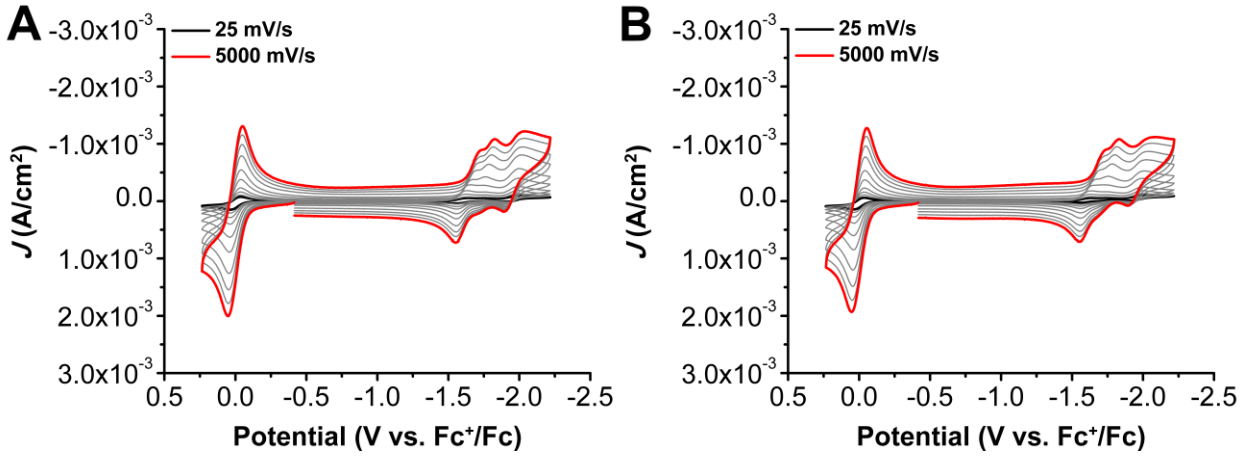

Figure S5. CVs of Cr($^{p\text{-}tbu}$dhbpy)Cl(H_2O) **1** at variable scan rates ranging from 25 (black) to 5000 (red) mV/s under Ar (**A**) and CO_2 (**B**) saturation conditions. Conditions: 1.0 mM **1**, 0.1 M $TBAPF_6$/DMF; glassy carbon disc working electrode, glassy carbon rod counter electrode, Ag/AgCl pseudoreference electrode; varied scan rate; referenced to internal ferrocene standard.

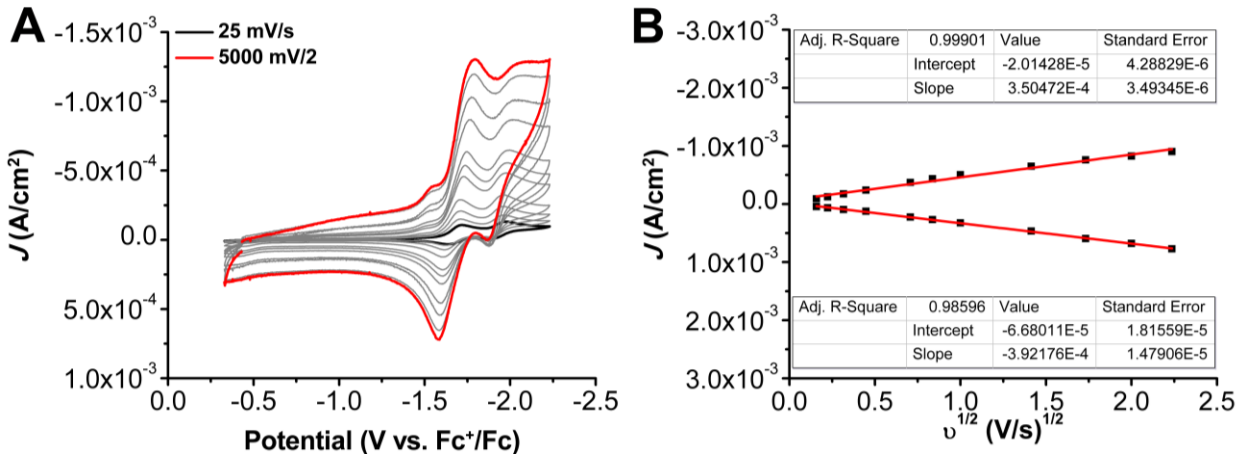

Figure S6. (**A**) CVs of Cr($^{p\text{-}tbu}$dhbpy)Cl(H_2O) **1** and excess TBACl at variable scan rates ranging from 25 (black) to 5000 (red) mV/s, obtained under Ar saturation conditions. (**B**) Linear Fit of variable scan rate data from (**A**) demonstrating that Cr($^{p\text{-}tbu}$dhbpy)Cl(H_2O) **1** shows a diffusion-limited current response. The data in (**B**) was obtained from the reversible redox feature at −1.69 V vs Fc^+/Fc. Conditions: 1.0 mM **1**, 0.1 M TBACl, and 0.1 M $TBAPF_6$/DMF; glassy carbon disc working electrode, glassy carbon rod counter electrode, Ag/AgCl pseudoreference electrode; varied scan rate; referenced to internal ferrocene standard.

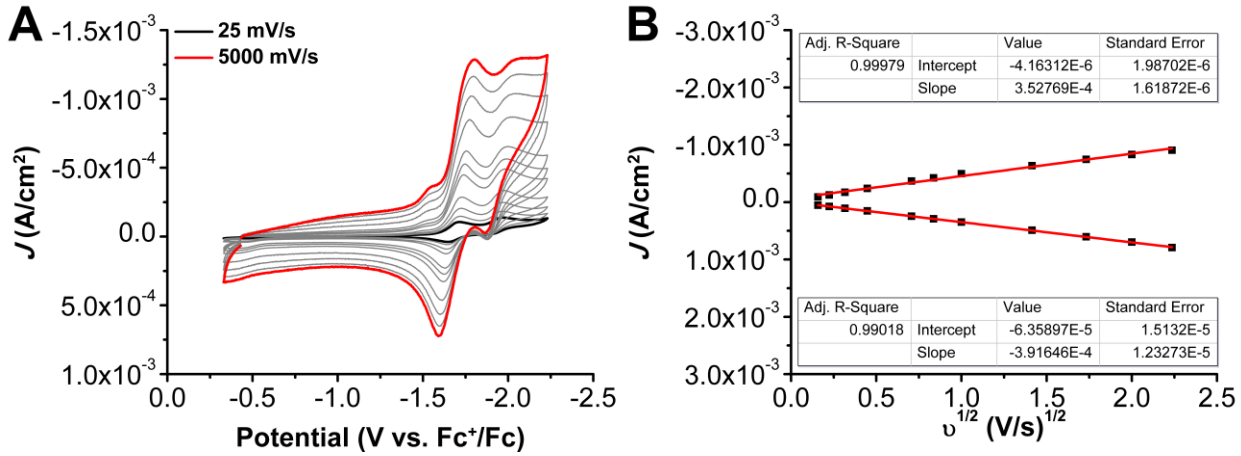

Figure S7. (**A**) CVs of Cr($^{p\text{-}tbu}$dhbpy)Cl(H_2O) **1** and excess TBACl at variable scan rates ranging from 25 (black) to 5000 (red) mV/s, obtained under CO_2 saturation conditions. (**B**) Linear Fit of variable scan rate data from (**A**) demonstrating that Cr($^{p\text{-}tbu}$dhbpy)Cl(H_2O) **1** shows a diffusion-limited current response. The data in (**B**) was obtained from the reversible redox feature at −1.66 V vs Fc^+/Fc. Conditions: 1.0 mM **1**, 0.1 M TBACL, and 0.1 M $TBAPF_6$/DMF; glassy carbon disc working electrode, glassy carbon rod counter electrode, Ag/AgCl pseudoreference electrode; varied scan rate; referenced to internal ferrocene standard.

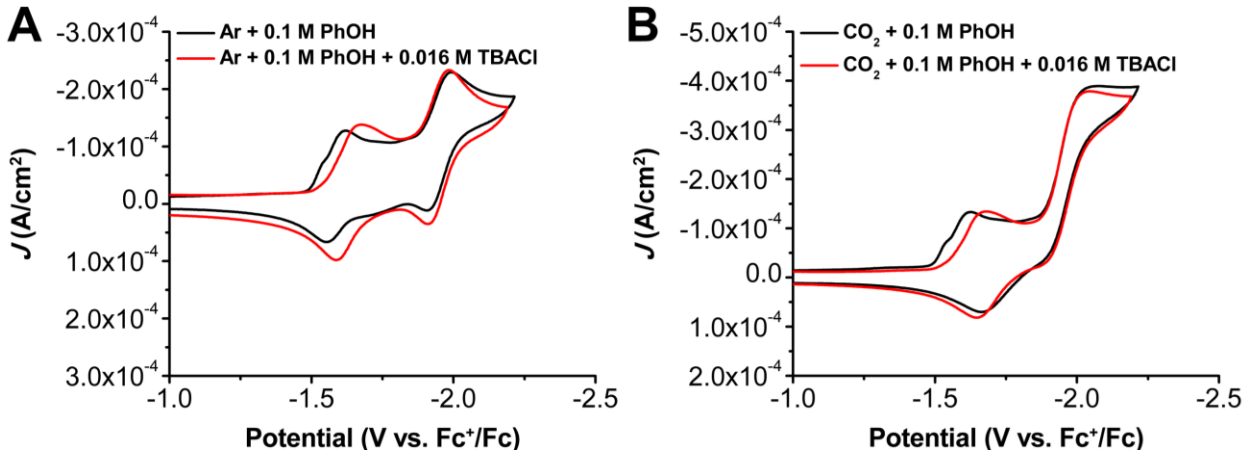

Figure S8. CVs of Cr($^{p\text{-}tbu}$dhbpy)Cl(H_2O) **1** and 0.1 M PhOH with and without added TBACl under Ar (**A**) or CO_2 (**B**) saturation conditions. Conditions: 1.0 mM **1**, 0.1 M $TBAPF_6$/DMF; glassy carbon disc working electrode, glassy carbon rod counter electrode, Ag/AgCl pseudoreference electrode; 100 mV/s scan rate; referenced to internal ferrocene standard.

For all variable concentration studies analysis was adapted from Sathrum and Kubiak *J. Phys. Chem. Lett.* **2011**, *2*, 2372.[25] *F* is Faraday's constant, *A* is the electrode area, [Q] is the substrate concentration, k_{cat} is the catalytic rate, *D* is the diffusion constant of the catalyst, [cat] is the concentration of the catalyst, and n_{cat} is the number of electrons involved in the catalytic process.

$$\boldsymbol{i_{cat} = n_{cat}FA[cat](Dk_{cat}[Q]^{y})^{1/2}}$$

For the variable acid and CO_2 concentration experiments, only points outside of the saturation range, where compatible S-shaped responses were observed, were analyzed.

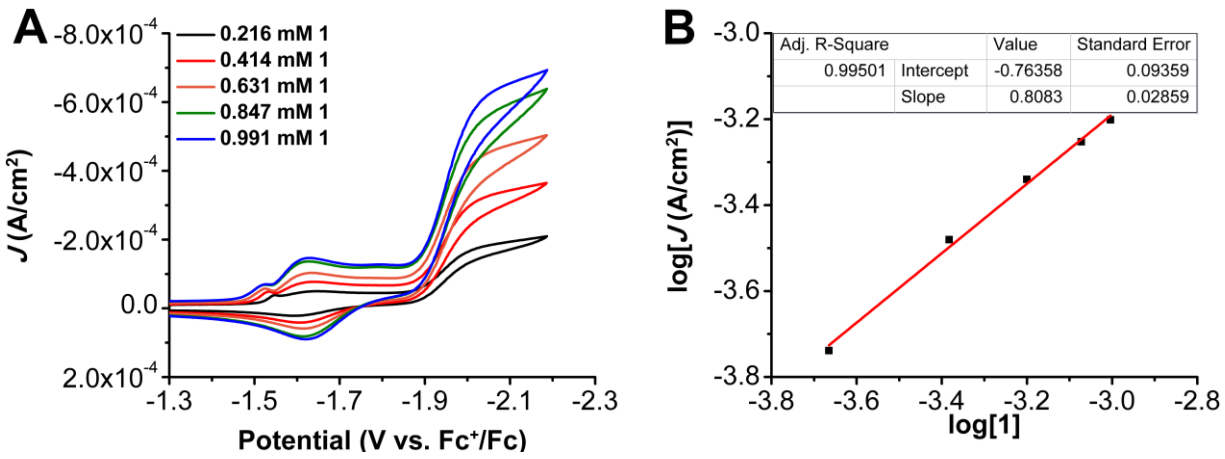

Figure S9. (**A**) CVs of Cr($^{p\text{-}tbu}$dhbpy)Cl(H_2O) **1** at variable concentrations, obtained under CO_2 saturation with 0.60 M PhOH. Conditions: 0.1 M $TBAPF_6$/DMF; glassy carbon disc working electrode, glassy carbon rod counter electrode, Ag/AgCl pseudoreference electrode; 100 mV/s scan rate; referenced to internal ferrocene standard. (**B**) Log-log plot from data obtained from CVs in **A** at −2.06 V vs. Fc^+/Fc.

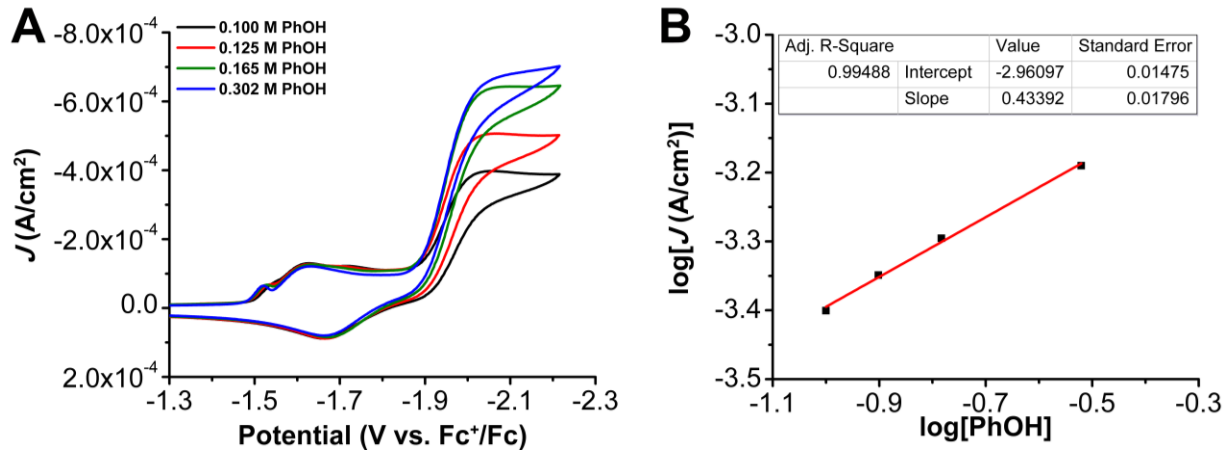

Figure S10. (**A**) CVs of 1.0 mM Cr($^{p\text{-}tbu}$dhbpy)Cl(H_2O) **1**, obtained under CO_2 saturation conditions with variable PhOH concentration.Conditions: 1.0 mM **1**, 0.1 M $TBAPF_6$/DMF; glassy carbon disc working electrode, glassy carbon rod counter electrode, Ag/AgCl pseudoreference electrode; 100 mV/s scan rate; referenced to internal ferrocene standard. (**B**) Log-log plot from data obtained from CVs in **A** at −2.06 V vs. Fc^+/Fc, only points outside of the saturation range were included in the linear fits.

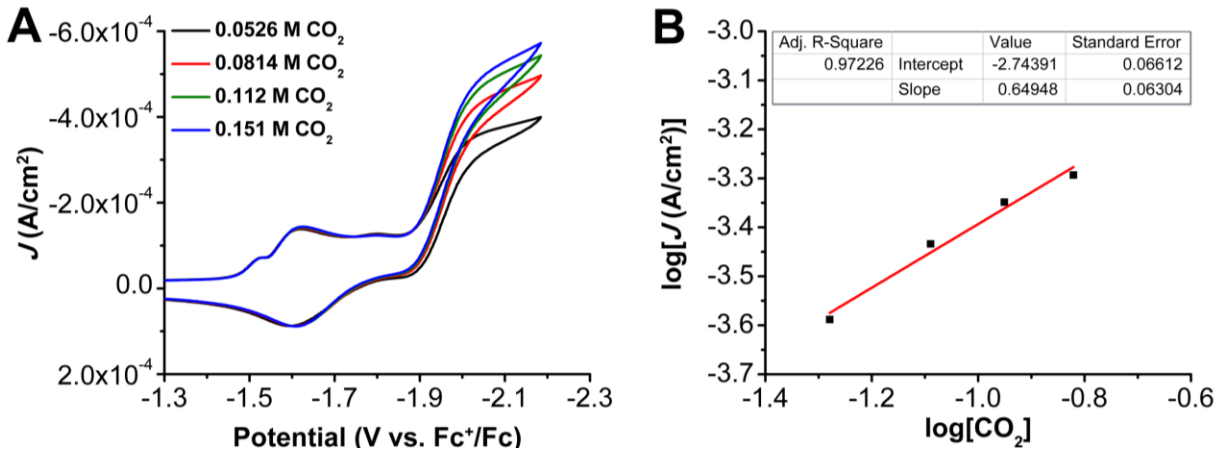

Figure S11. (**A**) CVs of 1.0 mM Cr($^{p\text{-}tbu}$dhbpy)Cl(H_2O) **1** obtained under variable CO_2 concentration with 0.60 M PhOH. Conditions: 0.1 M $TBAPF_6$/DMF; glassy carbon disc working electrode, glassy carbon rod counter electrode, Ag/AgCl pseudoreference electrode; 100 mV/s scan rate; referenced to internal ferrocene standard. (**B**) Log–log plot from data obtained from CVs in **A** at −2.05 V vs. Fc^+/Fc, only points outside of the saturation range were included in the linear fits.

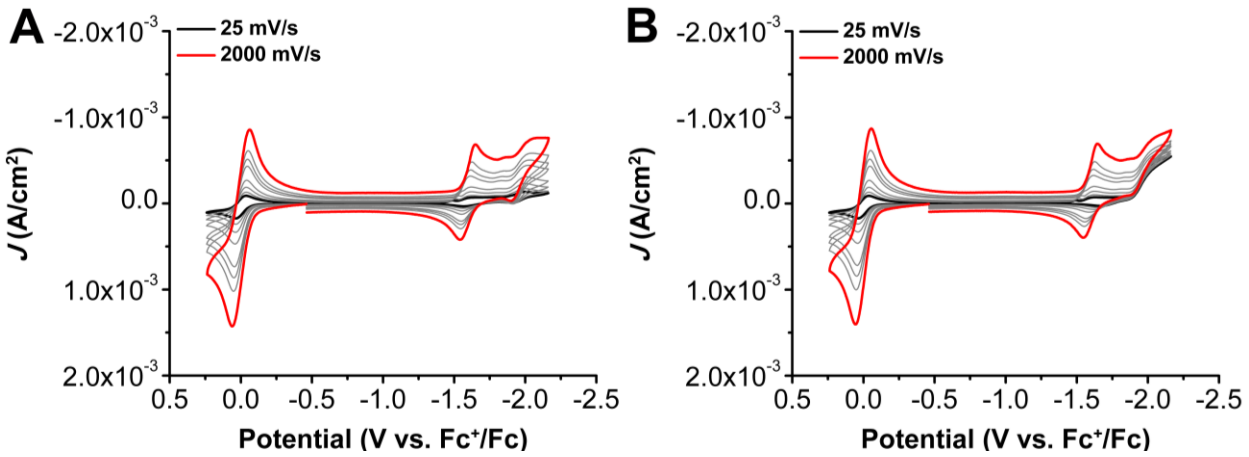

Figure S12. (A) CVs of Cr($^{p\text{-}tbu}$dhbpy)Cl(H_2O) **1** with 0.6 M PhOH at variable scan rates ranging from 25 (black) to 2000 (red) mV/s, obtained under Ar (**A**) and CO_2 (**B**) saturation conditions. Conditions 1.0 mM **1**, 0.1 M $TBAPF_6$/DMF; glassy carbon working electrode, glassy carbon counter electrode, Ag/AgCl pseudoreference electrode; varied scan rate; referenced to internal ferrocene standard.

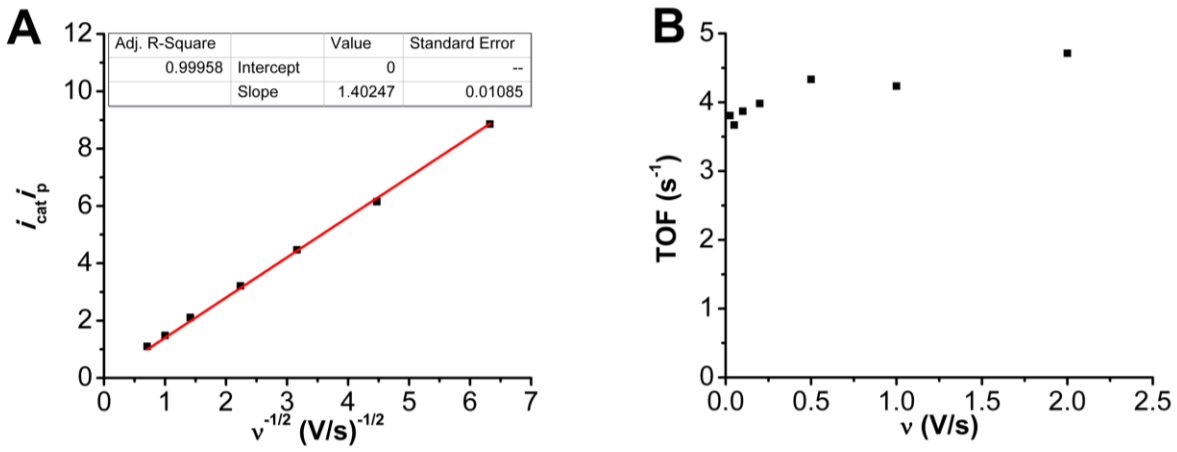

Figure S13. Plots of (**A**) i_{cat}/i_p versus the inverse of the square root of the scan rate and (**B**) TOF versus scan rate for 1.0 mM Cr($^{p\text{-tbu}}$dhbpy)Cl(H_2O) **1**, with 0.6 M PhOH from data in Figure **S12**.

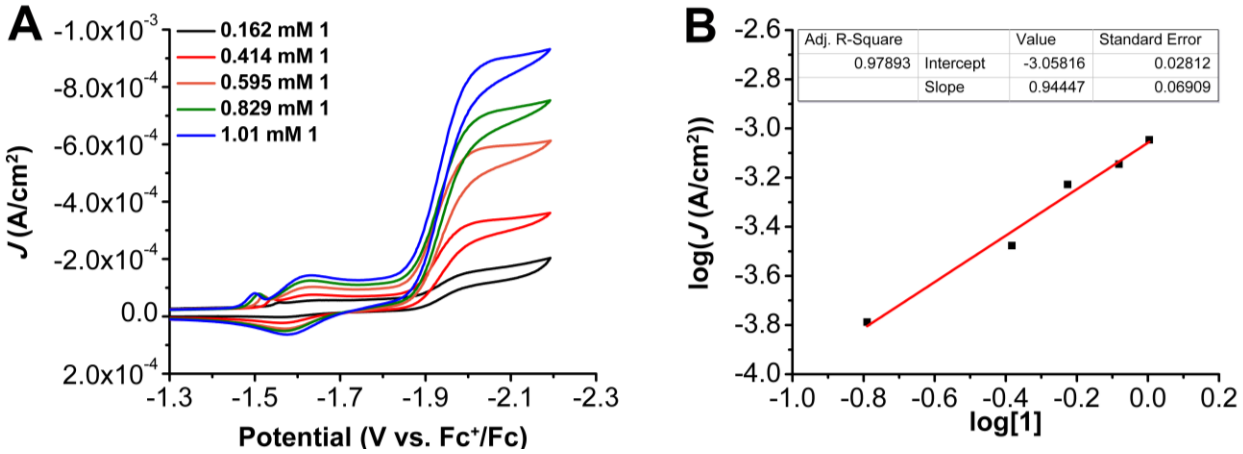

Figure S14. (**A**) CVs of Cr($^{p\text{-tbu}}$dhbpy)Cl(H_2O) **1** at variable concentrations, obtained under CO_2 saturation with 1.0 M TFE. Conditions: 0.1 M $TBAPF_6$/DMF; glassy carbon disc working electrode, glassy carbon rod counter electrode, Ag/AgCl pseudoreference electrode; 100 mV/s scan rate; referenced to internal ferrocene standard. (**B**) Log-log plot from data obtained from CVs in **A** at −2.04 V vs. Fc^+/Fc.

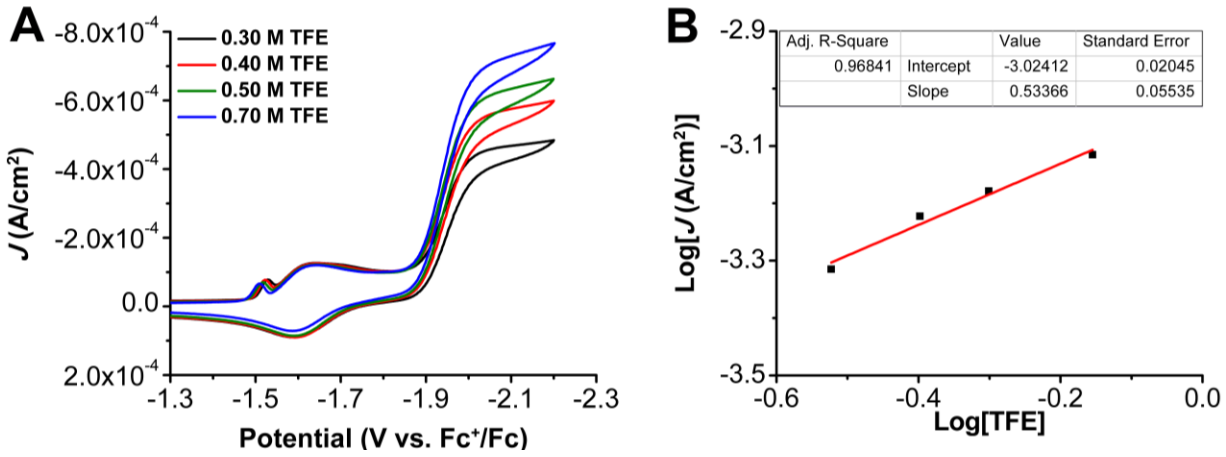

Figure S15. (**A**) CVs of 1.0 mM Cr($^{p\text{-}tbu}$dhbpy)Cl(H_2O) **1**, obtained under CO_2 saturation conditions with variable TFE concentration.Conditions: 1.0 mM **1**, 0.1 M $TBAPF_6$/DMF; glassy carbon disc working electrode, glassy carbon rod counter electrode, Ag/AgCl pseudoreference electrode; 100 mV/s scan rate; referenced to internal ferrocene standard. (**B**) Log-log plot from data obtained from CVs in **A** at −2.03 V vs. Fc^+/Fc, only points outside of the saturation range were included in the linear fits.

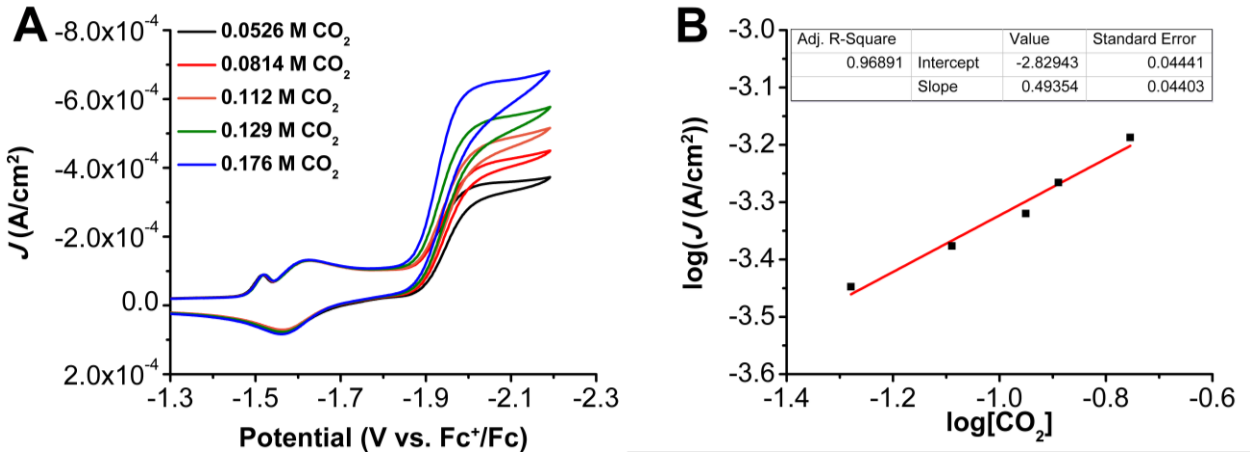

Figure S16. (**A**) CVs of 1.0 mM Cr($^{p\text{-}tbu}$dhbpy)Cl(H_2O) **1** obtained under variable CO_2 concentration with 1.0 M TFE. Conditions: 0.1 M $TBAPF_6$/DMF; glassy carbon disc working electrode, glassy carbon rod counter electrode, Ag/AgCl pseudoreference electrode; 100 mV/s scan rate; referenced to internal ferrocene standard. (**B**) Log-log plot from data obtained from CVs in **A** at −2.06 V vs. Fc^+/Fc, only points outside of the saturation range were included in the linear fits.

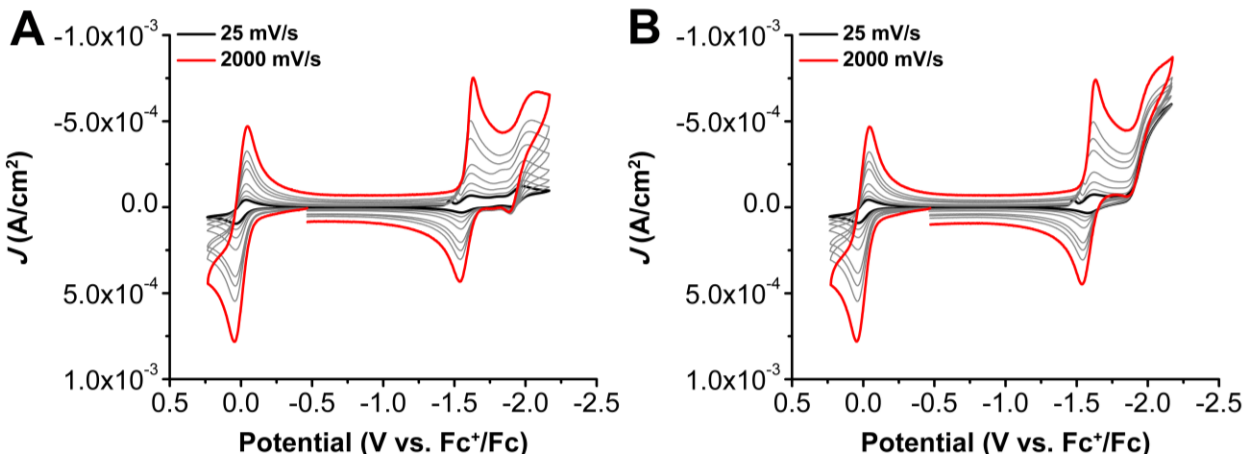

Figure S17. (**A**) CVs of Cr($^{p\text{-}tbu}$dhbpy)Cl(H_2O) **1** with 1.0 M TFE at variable scan rates ranging from 25 (black) to 2000 (red) mV/s, obtained under Ar (**A**) and CO_2 (**B**) saturation conditions. Conditions 1.0 mM **1**, 0.1 M $TBAPF_6$/DMF; glassy carbon working electrode, glassy carbon counter electrode, Ag/AgCl pseudoreference electrode; varied scan rate; referenced to internal ferrocene standard.

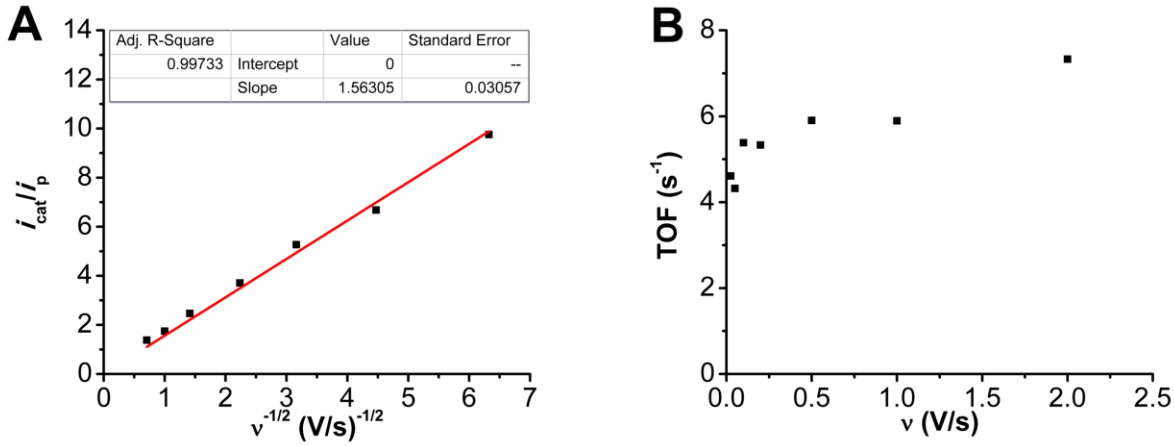

Figure S18. Plots of (**A**) i_{cat}/i_p versus the inverse of the square root of the scan rate and (**B**) TOF versus scan rate for 1.0 mM Cr($^{p\text{-}tbu}$dhbpy)Cl(H_2O) **1**, with 1.0 M TFE from data in Figure **S17**.

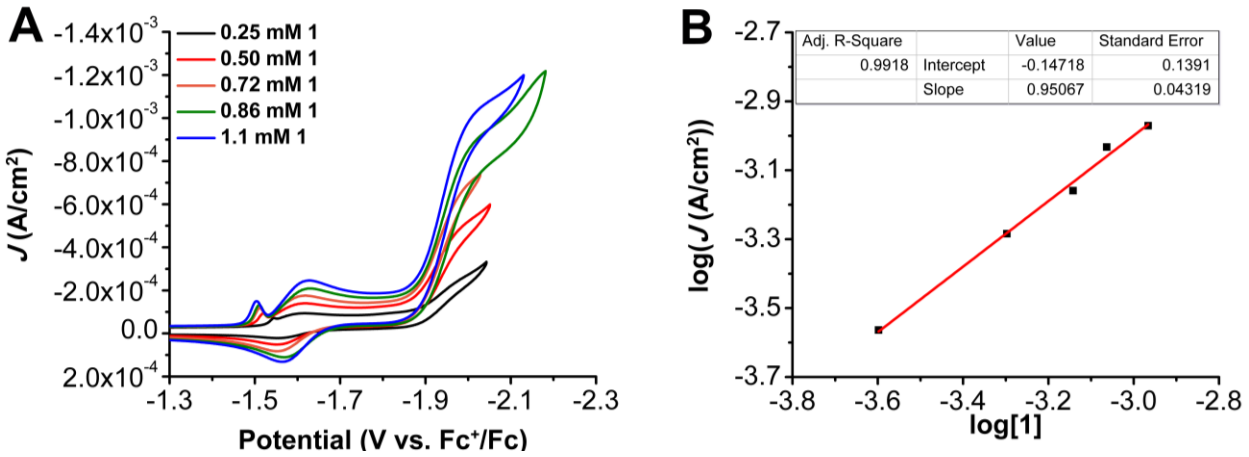

Figure S19. (**A**) CVs of Cr($^{p\text{-}tbu}$dhbpy)Cl(H_2O) **1** at variable concentrations, obtained under CO_2 saturation with 20 mM $TEAHPF_6$. Conditions: 0.1 M $TBAPF_6$/DMF; glassy carbon disc working electrode, glassy carbon rod counter electrode, Ag/AgCl pseudoreference electrode; 100 mV/s scan rate; referenced to internal ferrocene **A** standard. (**B**) Log-log plot from data obtained from CVs in **A** at −2.00 V vs. Fc^+/Fc.

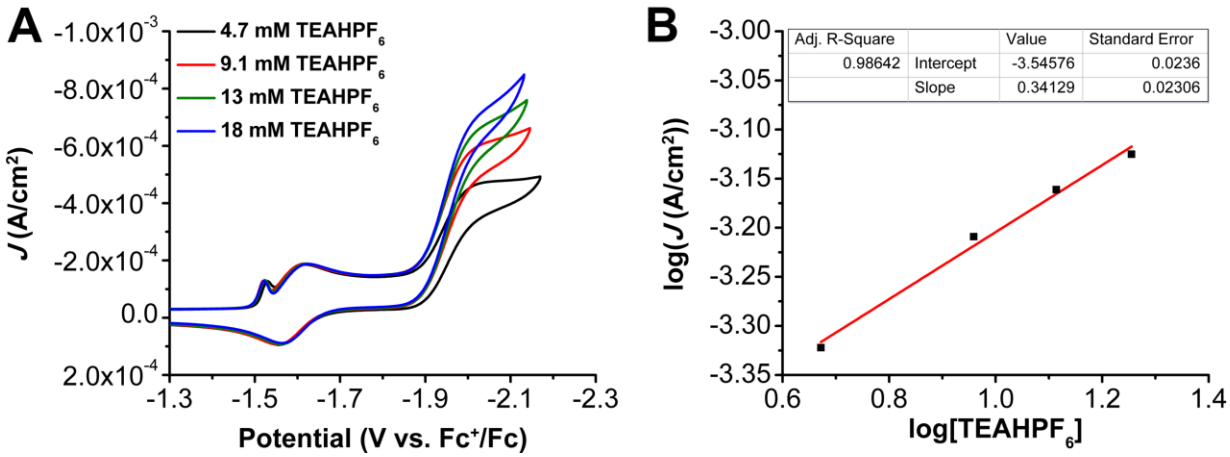

Figure S20. (**A**) CVs of 1.0 mM Cr($^{p\text{-}tbu}$dhbpy)Cl(H_2O) **1**, obtained under CO_2 saturation conditions with variable $TEAHPF_6$ concentration.Conditions: 1.0 mM **1**, 0.1 M $TBAPF_6$/DMF; glassy carbon disc working electrode, glassy carbon rod counter electrode, Ag/AgCl pseudoreference electrode; 100 mV/s scan rate; referenced to internal ferrocene standard. (**B**) Log-log plot from data obtained from CVs in **A** at −2.06 V vs. Fc^+/Fc, only points outside of the saturation range were included in the linear fits.

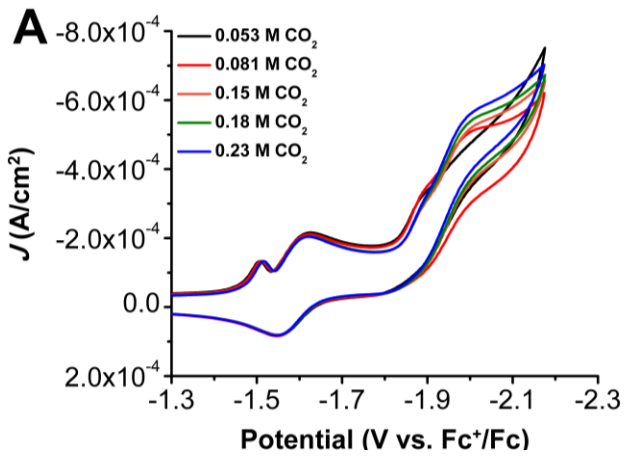

Figure S21. (**A**) CVs of 1.0 mM Cr($^{p\text{-}tbu}$dhbpy)Cl(H_2O) **1** obtained under variable CO_2 concentration with 20 mM TEAHPF_6. Conditions: 0.1 M TBAPF_6/DMF; glassy carbon disc working electrode, glassy carbon rod counter electrode, Ag/AgCl pseudoreference electrode; 100 mV/s scan rate; referenced to internal ferrocene standard. Log–log plot from data was not obtained from CVs in **A** as there is competing HER occurring at low concentrations of CO_2.

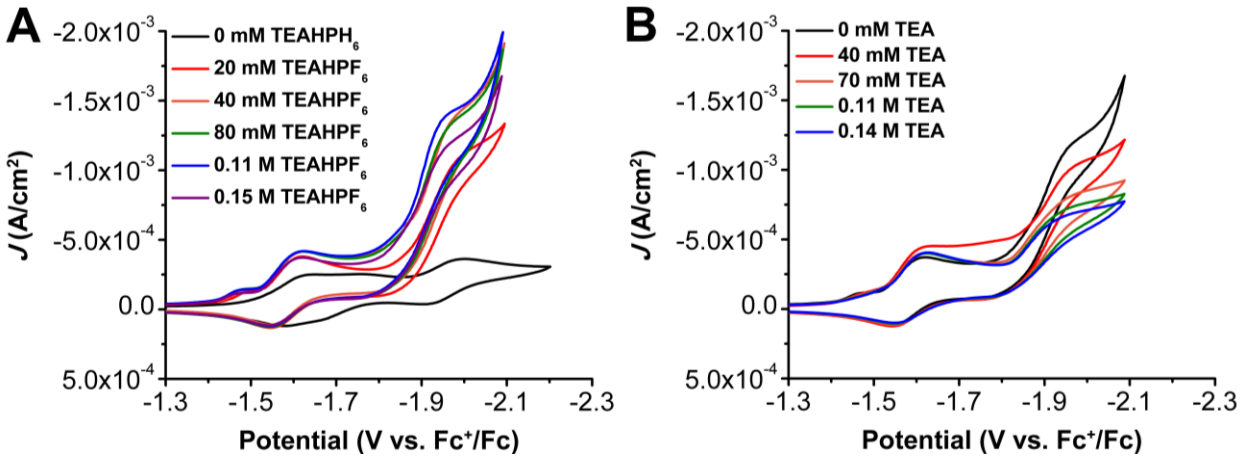

Figure S22. (**A**) CVs of 1.0 mM Cr($^{p\text{-}tbu}$dhbpy)Cl(H_2O) **1**, obtained under CO_2 saturation conditions with variable TEAHPF_6 concentration. Conditions: 1.0 mM **1**, 0.1 M TBAPF_6/DMF; glassy carbon disc working electrode, glassy carbon rod counter electrode, Ag/AgCl pseudoreference electrode; 100 mV/s scan rate; referenced to internal ferrocene standard. (**B**) CVs of 1.0 mM Cr($^{p\text{-}tbu}$dhbpy)Cl(H_2O) **1** and 0.15 M TEAHPF_6 obtained under CO_2 saturation conditions with variable TEA concentration. Conditions: 0.15 M TEAHPF_6 and 1.0 mM **1**, 0.1 M TBAPF_6/DMF; glassy carbon disc working electrode, glassy carbon rod counter electrode, Ag/AgCl pseudoreference electrode; 100 mV/s scan rate; referenced to internal ferrocene standard.

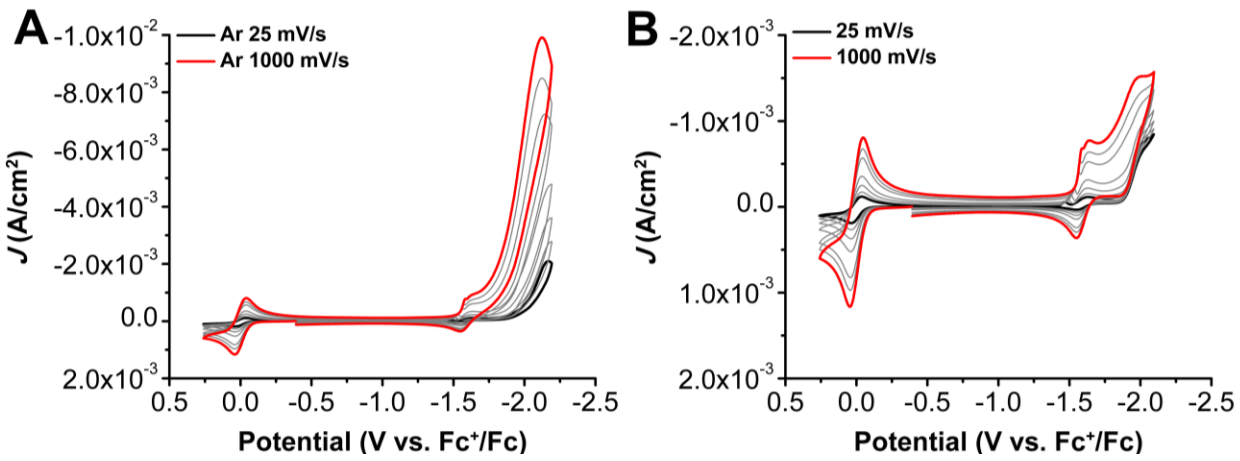

Figure S23. (**A**) CVs of Cr($^{p\text{-}tbu}$dhbpy)Cl(H_2O) **1** with 20 mM $TEAHPF_6$ at variable scan rates ranging from 25 (black) to 1000 (red) mV/s, obtained under Ar (**A**) and CO_2 (**B**) saturation conditions. Conditions 1.0 mM **1**, 0.1 M $TBAPF_6$/DMF; glassy carbon working electrode, glassy carbon counter electrode, Ag/AgCl pseudoreference electrode; varied scan rate; referenced to internal ferrocene standard.

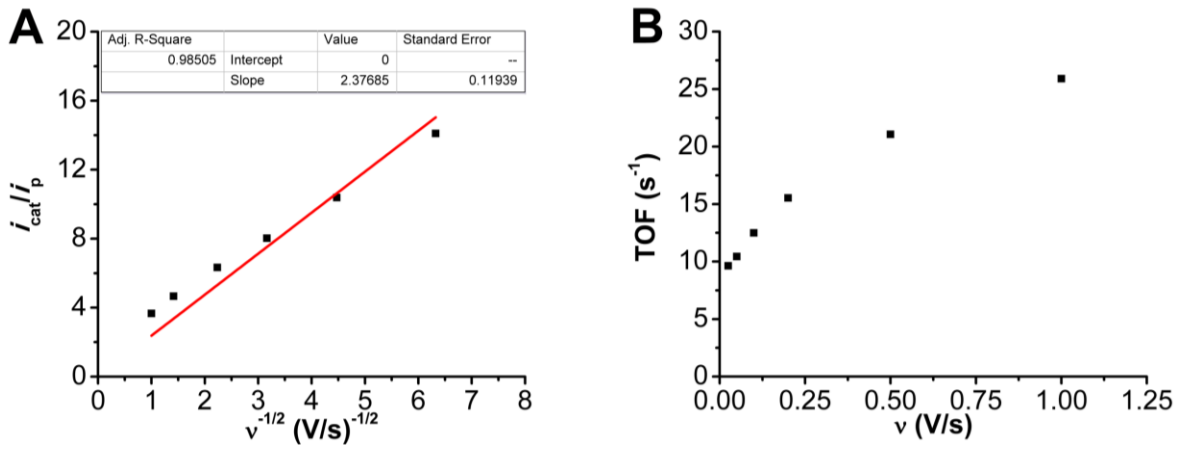

Figure S24. Plots of (**A**) i_{cat}/i_p versus the inverse of the square root of the scan rate and (**B**) TOF versus scan rate for 1.0 mM Cr($^{p\text{-}tbu}$dhbpy)Cl(H_2O) **1**, with 20 mM $TEAHPF_6$ from data in Figure **S23**. The trend away from zero-zero intercept is consistent with contributions from a heterogeneous HER response.

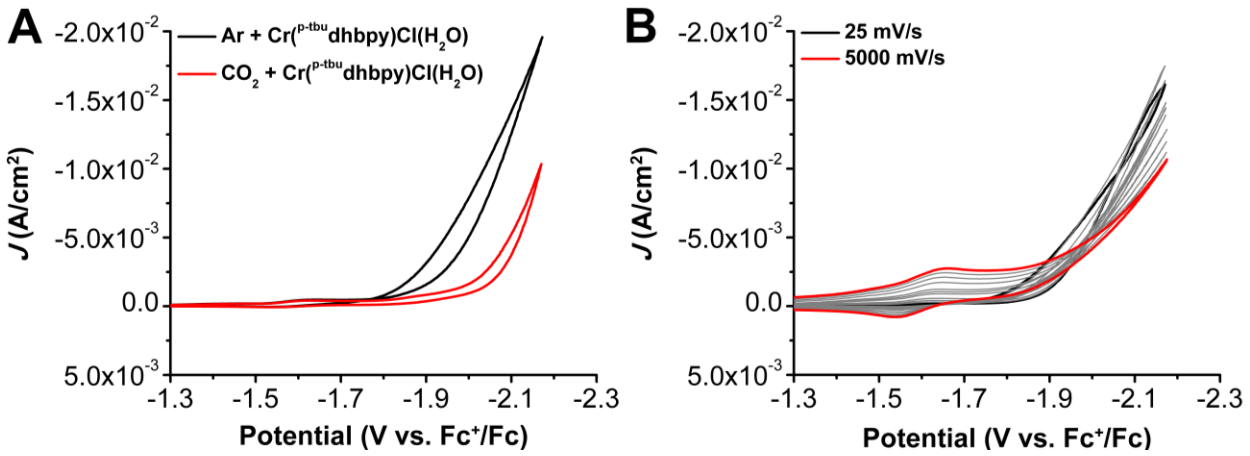

Figure S25. (**A**) CVs of 1.0 mM Cr($^{p\text{-}tbu}$dhbpy)Cl(H_2O) **1**, obtained under Ar and CO_2 saturation conditions. (**B**) CVs of 1.0 mM Cr($^{p\text{-}tbu}$dhbpy)Cl(H_2O) **1**, obtained under Ar saturation conditions at variable scan rates.Conditions: 1.0 mM **1**, 0.1 M $TEAHPF_6$/DMF; glassy carbon disc working electrode, glassy carbon rod counter electrode, Ag/AgCl pseudoreference electrode; 100 mV/s scan rate; referenced to internal ferrocene standard.

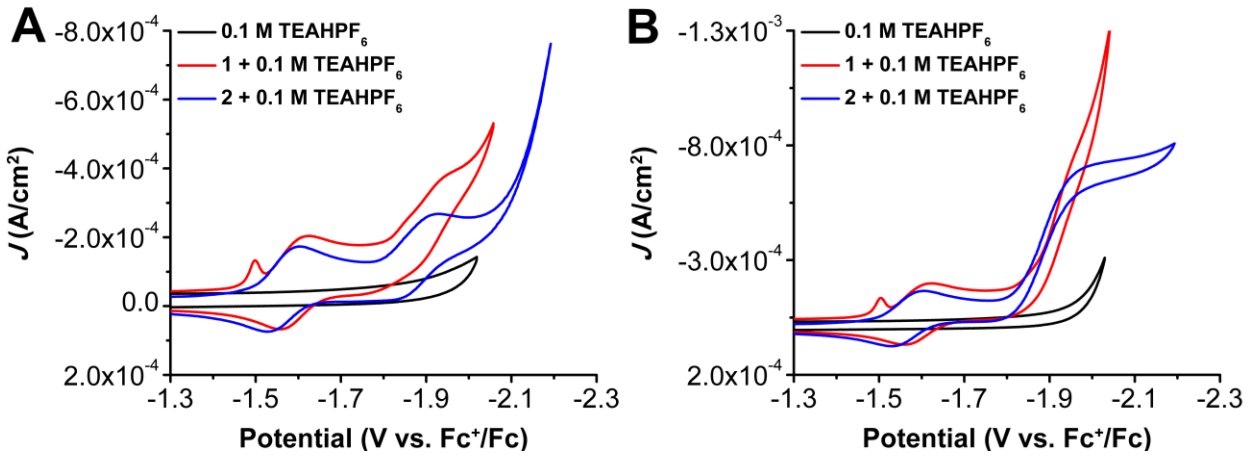

Figure S26. (**A**) CVs of 0.1 M $TEAHPF_6$, overlayed with 1.0 mM Cr($^{p\text{-}tbu}$dhbpy)Cl(H_2O) **1** and 1.0 mM Cr(^{nPr}dhbpy)Cl(H_2O) **2** with 0.1 M $TEAHPF_6$ under Ar (**A**) and CO_2 (**B**) saturation conditions. Conditions: 1.0 mM catalyst, 0.1 M $TBAPF_6$/DMF; glassy carbon disc working electrode, glassy carbon rod counter electrode, Ag/AgCl pseudoreference electrode; 100 mV/s scan rate; referenced to internal ferrocene standard.

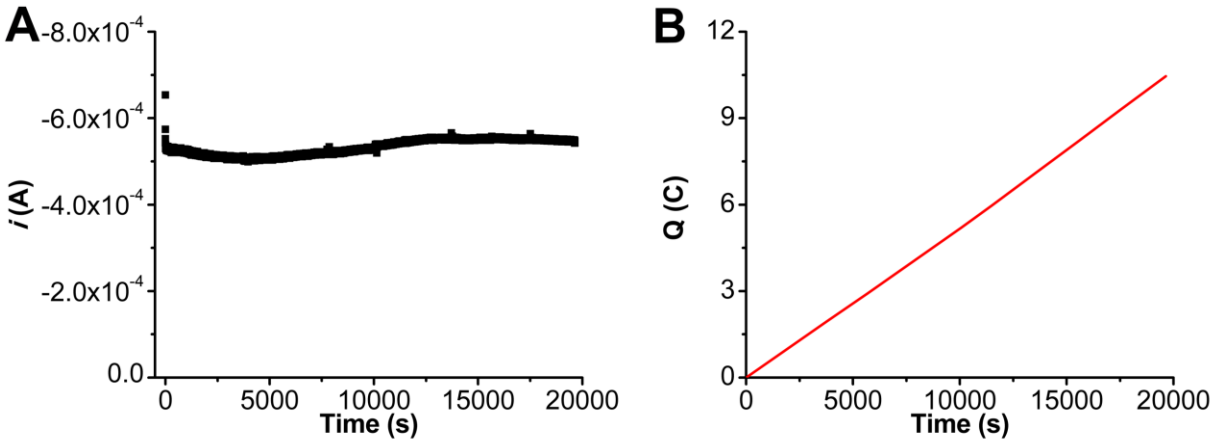

Figure S27. (**A**) Current versus time trace from CPE experiment for **1** + PhOH. (**B**) Charge passed versus time for the CPE experiment shown in **A**. Conditions were 0.75 mM Cr($^{p\text{-}tbu}$dhbpy)Cl(H_2O) **1** and 1.5 M PhOH under a CO_2 atmosphere at −2.10 V vs Fc^+/Fc in 0.1 M $TBAPF_6$/DMF; working electrode was a glassy carbon rod, counter electrode was a graphite rod, and the reference was a nonaqueous Ag/AgCl pseudoreference electrode; 0.075 M Fc was used as sacrificial oxidant.

Table S4. Results from CPE experiment in **Figure S27**, 0.75 mM **1** + 1.5 M PhOH.

Time (s)	Charge (coulombs)	moles (e^-)	Moles of CO	FE_{CO}	FE_{H2}
19646*	10.5	1.08×10^{-4}	4.27×10^{-5}	78.85	4.63
19646*	10.5	1.08×10^{-4}	4.87×10^{-5}	89.80	5.73
19646*	10.5	1.08×10^{-4}	4.86×10^{-5}	89.74	5.33
19646*	10.5	1.08×10^{-4}	4.45×10^{-5}	82.16	4.75

* indicates a series of injections carried out upon completion of electrolysis.

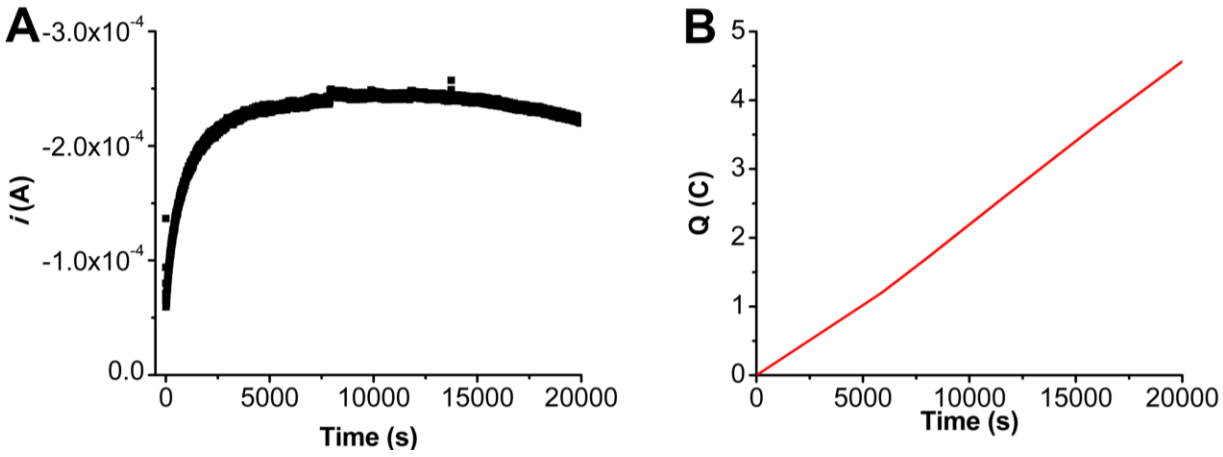

Figure S28. (**A**) Current versus time trace from rinse test of CPE experiment in **Figure S27** (**B**) Charge passed versus time for the CPE experiment shown in **A**. Conditions were 1.5 M PhOH under a CO_2 atmosphere at −2.1 V vs Fc^+/Fc in 0.1 M $TBAPF_6$/DMF; working electrode was the glassy carbon rod used in the experiment shown in **Figure S27** that was rinsed with DMF and not polished, counter electrode was a graphite rod, and the reference was a nonaqueous Ag/AgCl pseudoreference electrode; 0.075 M Fc was used as sacrificial oxidant.

Table S5. Results from CPE experiment in **Figure S28**.

Time (s)	Charge (coulombs)	moles (e^-)	Moles of CO	Moles of H_2
20059*	4.58	4.75×10^{-5}	<LOQ	6.87×10^{-6}
20059*	4.58	4.75×10^{-5}	<LOQ	7.14×10^{-6}
20059*	4.58	4.75×10^{-5}	<LOQ	6.28×10^{-6}

* indicates a triplicate series of injections carried out upon completion of electrolysis.

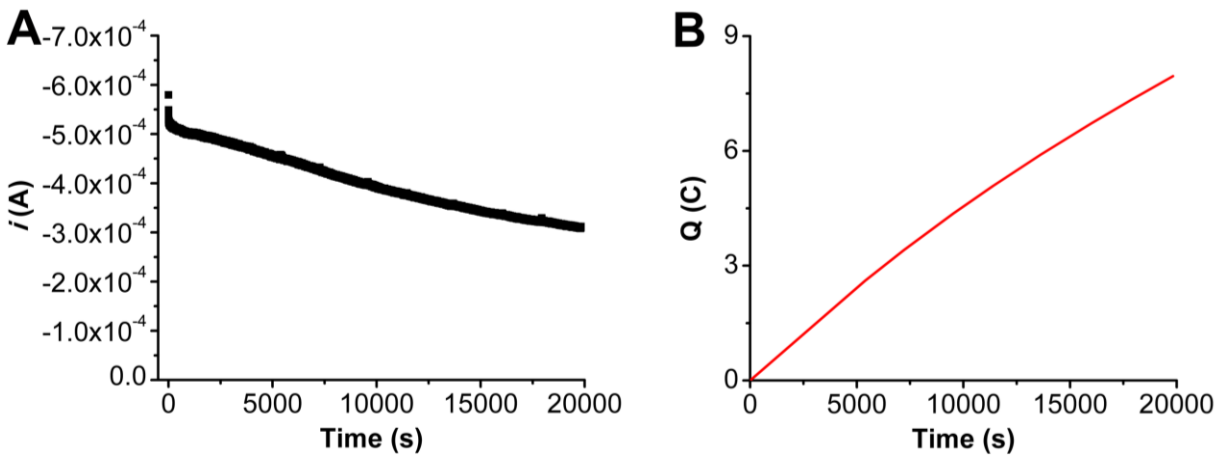

Figure S29. (**A**) Current versus time trace from CPE experiment for **1** + TFE. (**B**) Charge passed versus time for the CPE experiment shown in **A**. Conditions were 0.5 mM Cr($^{p\text{-}tbu}$dhbpy)Cl(H_2O) **1** and 1.0 M TFE under a CO_2 atmosphere at −2.10 V vs Fc^+/Fc in 0.1 M $TBAPF_6$/DMF; working electrode was a glassy carbon rod, counter electrode was a graphite rod, and the reference was a nonaqueous Ag/AgCl pseudoreference electrode; 0.075 M Fc was used as sacrificial oxidant.

Table S6. Results from CPE experiment in **Figure S29**, 0.5 mM **1** + 1.0 M TFE.

Time (s)	Charge (coulombs)	moles (e^-)	Moles of CO	FE$_{CO}$
19831*	7.96	8.25 x 10^{-5}	4.21 x 10^{-5}	102
19831*	7.96	8.25 x 10^{-5}	4.38 x 10^{-5}	106
19831*	7.96	8.25 x 10^{-5}	4.27 x 10^{-5}	104
19831*	7.96	8.25 x 10^{-5}	4.06 x 10^{-5}	98.5

* indicates a series of injections carried out upon completion of electrolysis.

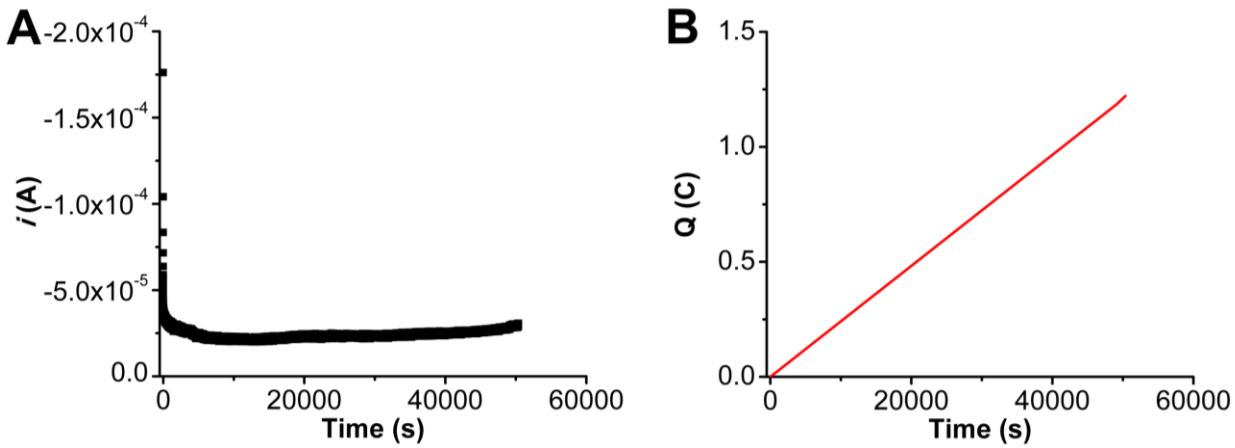

Figure S30. (**A**) Current versus time trace from rinse test of CPE experiment in **Figure S29** (**B**) Charge passed versus time for the CPE experiment shown in **A**. Conditions were 1.0 M TFE under a CO_2 atmosphere at −2.1 V vs Fc^+/Fc in 0.1 M $TBAPF_6$/DMF; working electrode was the glassy carbon rod used in the experiment shown in **Figure S29** that was rinsed with DMF and not polished, counter electrode was a graphite rod, and the reference was a nonaqueous Ag/AgCl pseudoreference electrode; 0.075 M Fc was used as sacrificial oxidant.

Table S7. Results from CPE experiment in **Figure S30**.

Time (s)	Charge (coulombs)	moles (e^-)	Moles of CO	Moles of H_2
50367*	1.22	1.27 x 10^{-5}	<LOQ	<LOQ
50367*	1.22	1.27 x 10^{-5}	<LOQ	<LOQ
50367*	1.22	1.27 x 10^{-5}	<LOQ	<LOQ

* indicates a triplicate series of injections carried out upon completion of electrolysis.

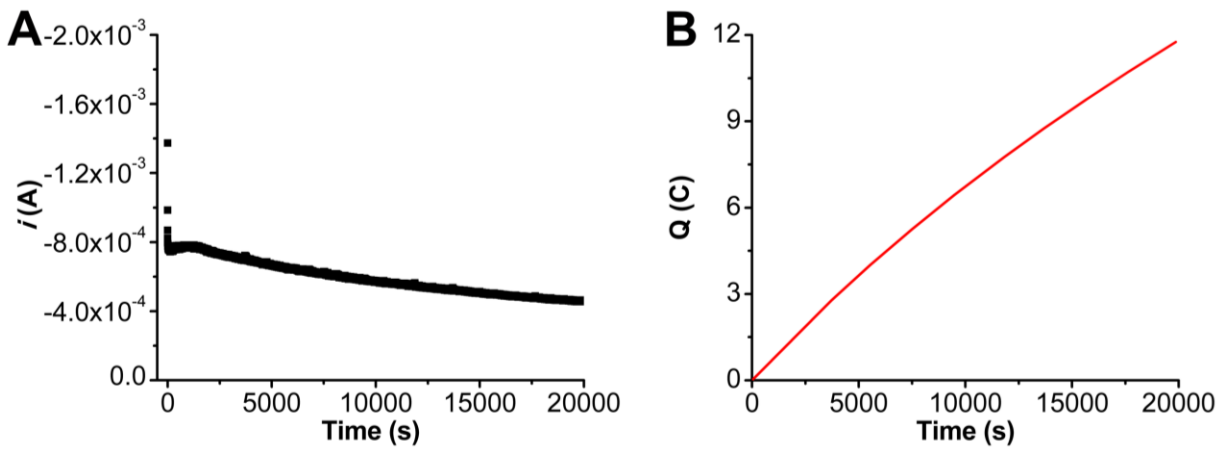

Figure S31. (**A**) Current versus time trace from CPE experiment for **1** + $TEAHPF_6$. (**B**) Charge passed versus time for the CPE experiment shown in **A**. Conditions were 0.5 mM Cr($^{p\text{-}tbu}$dhbpy)Cl(H_2O) (**1**), 20 mM $TEAHPF_6$ under a CO_2 atmosphere at −2.1 V vs Fc^+/Fc in 0.1 M $TBAPF_6$/DMF; working electrode was a graphite rod, counter electrode was a graphite rod, and the reference was a nonaqueous Ag/AgCl pseudoreference electrode; 0.075 M Fc was used as sacrificial oxidant.

Table S8. Results from CPE experiment in **Figure S31**, 0.5 mM **1** + 20 mM $TEAHPF_6$.

Time (s)	Charge (coulombs)	moles (e^-)	Moles of CO	FE_{CO}	FE_{H2}
19860*	11.8	1.22×10^{-4}	4.98×10^{-5}	81.81	17.55
19860*	11.8	1.22×10^{-4}	5.16×10^{-5}	84.67	17.56
19860*	11.8	1.22×10^{-4}	5.08×10^{-5}	83.43	17.68
19860*	11.8	1.22×10^{-4}	4.95×10^{-5}	81.26	16.95

* indicates a series of injections carried out upon completion of electrolysis

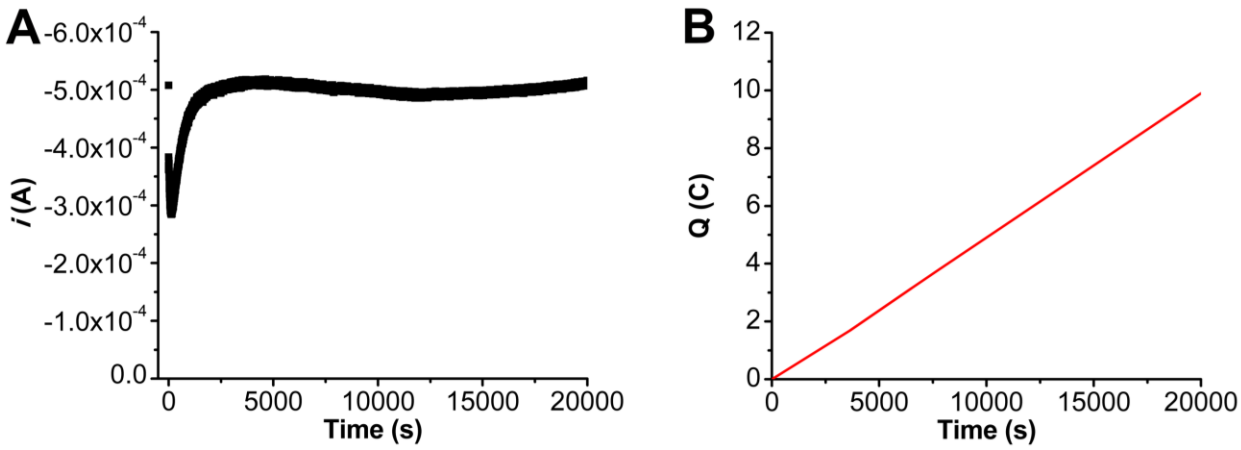

Figure S32. (**A**) Current versus time trace from rinse test of CPE experiment in **Figure S31** (**B**) Charge passed versus time for the CPE experiment shown in **A**. Conditions were 20 mM $TEAHPF_6$ under a CO_2 atmosphere at −2.1 V vs Fc^+/Fc in 0.1 M $TBAPF_6$/DMF; working electrode was the glassy carbon rod used in the experiment shown in **Figure S31** that was rinsed with DMF and not polished, counter electrode was a graphite rod, and the reference was a nonaqueous Ag/AgCl pseudoreference electrode; 0.075 M Fc was used as sacrificial oxidant.

Table S9. Results from CPE experiment in **Figure S32**.

Time (s)	Charge (coulombs)	moles (e^-)	Moles of CO	Moles of H_2
21035*	10.4	1.08×10^{-4}	<LOQ	3.82×10^{-5}
21035*	10.4	1.08×10^{-4}	<LOQ	3.97×10^{-5}
21035*	10.4	1.08×10^{-4}	<LOQ	3.87×10^{-5}

* indicates a triplicate series of injections carried out upon completion of electrolysis.

Electrochemistry of 2

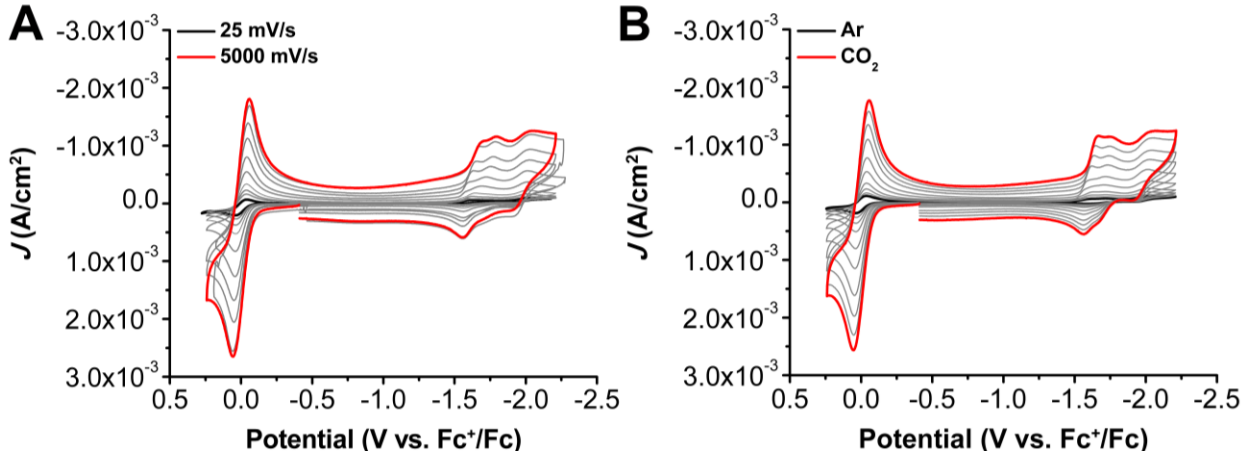

Figure S33. CVs of Cr(^{nPr}dhbpy)Cl(H_2O) **2** at variable scan rates ranging from 25 (black) to 5000 (red) mV/s under Ar (**A**) and CO_2 (**B**) saturation conditions. Conditions: 1.0 mM **2**, 0.1 M $TBAPF_6$/DMF; glassy carbon disc working electrode, glassy carbon rod counter electrode, Ag/AgCl pseudoreference electrode; varied scan rate; referenced to internal ferrocene standard.

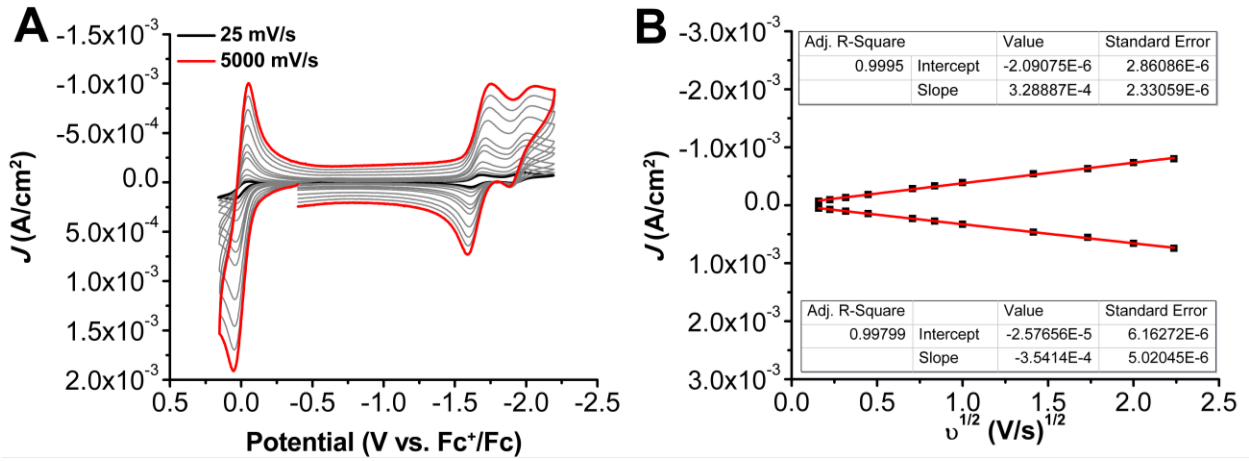

Figure S34. (**A**) CVs of Cr(^{nPr}dhbpy)Cl(H_2O) **2** at variable scan rates ranging from 25 (black) to 5000 (red) mV/s, obtained with excess TBACl and under Ar saturation conditions. (**B**) Linear Fit of variable scan rate data from **A** demonstrating that Cr(^{nPr}dhbpy)Cl(H_2O) **2** shows a diffusion-limited current response. The data in **B** was obtained from the reversible redox feature at −1.69 V vs Fc^+/Fc. Conditions: 1.0 mM **2**, 0.1 M TBACl, 0.1 M $TBAPF_6$/DMF; glassy carbon disc working electrode, glassy carbon rod counter electrode, Ag/AgCl pseudoreference electrode; varied scan rate; referenced to internal ferrocene standard.

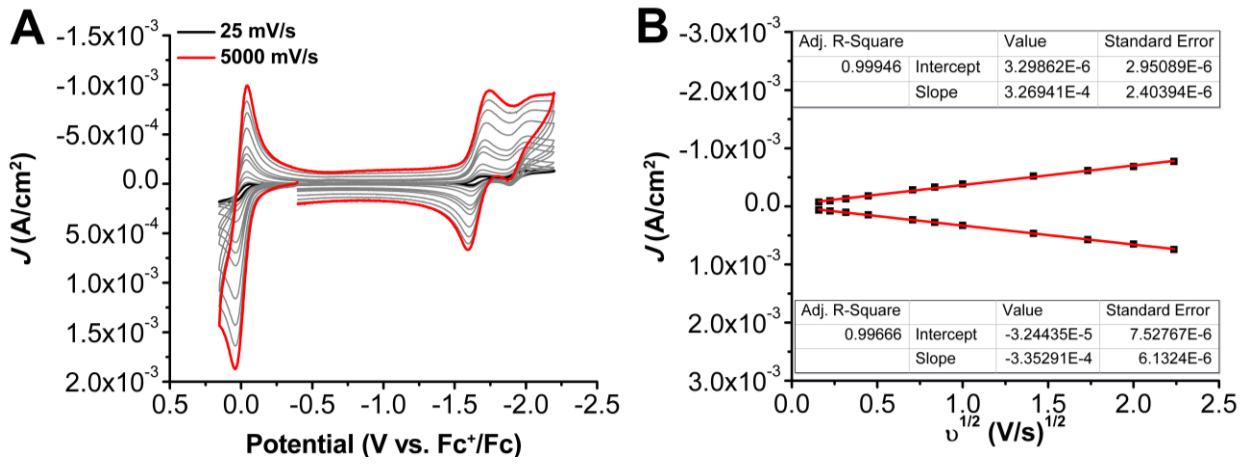

Figure S35. (**A**) CVs of Cr(^{nPr}dhbpy)Cl(H_2O) **2** at variable scan rates ranging from 25 (black) to 5000 (red) mV/s, obtained with excess TBACl and under CO_2 saturation conditions. (**B**) Linear Fit of variable scan rate data from **A** demonstrating that Cr(^{nPr}dhbpy)Cl(H_2O) **2** shows a diffusion-limited current response. The data in **B** was obtained from the reversible redox feature at −1.66 V vs Fc^+/Fc. Conditions: 1.0 mM **2**, 0.1 M TBACl, and 0.1 M $TBAPF_6$/DMF; glassy carbon disc working electrode, glassy carbon rod counter electrode, Ag/AgCl pseudoreference electrode; varied scan rate; referenced to internal ferrocene standard.

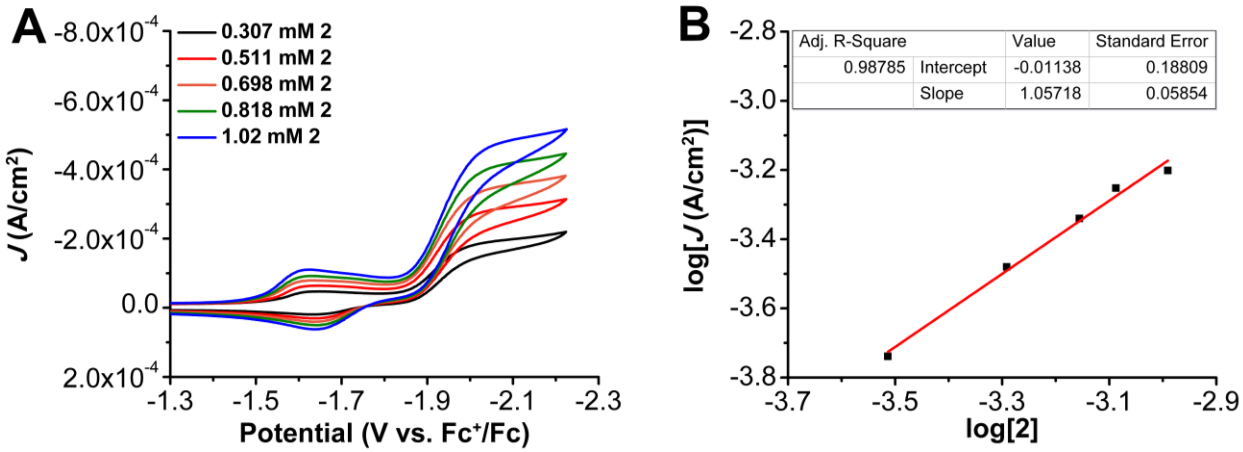

Figure S36. (**A**) CVs of Cr(^{nPr}dhbpy)Cl(H_2O) **2** at variable concentrations, obtained under CO_2 saturation with 0.60 M PhOH. Conditions: 0.1 M $TBAPF_6$/DMF; glassy carbon disc working electrode, glassy carbon rod counter electrode, Ag/AgCl pseudoreference electrode; 100 mV/s scan rate; referenced to internal ferrocene standard. (**B**) Log-log plot from data obtained from CVs in **A** at −2.01 V vs. Fc^+/Fc.

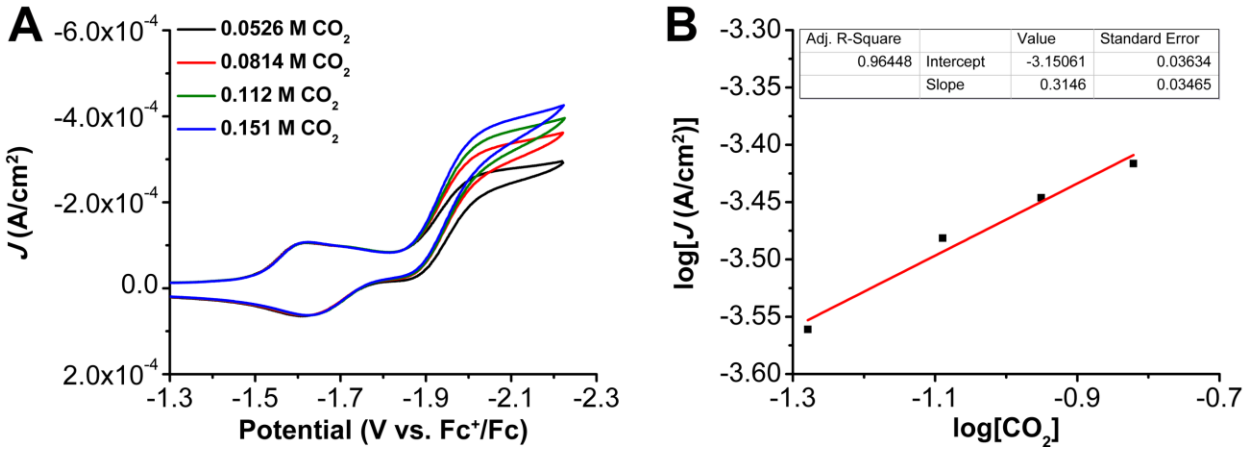

Figure S37. (**A**) CVs of 1.0 mM Cr(^{nPr}dhbpy)Cl(H_2O) **2** obtained under variable CO_2 concentration with 0.60 M PhOH. Conditions: 0.1 M $TBAPF_6$/DMF; glassy carbon disc working electrode, glassy carbon rod counter electrode, Ag/AgCl pseudoreference electrode; 100 mV/s scan rate; referenced to internal ferrocene standard. (**B**) Log–log plot from data obtained from CVs in **A** at −2.07 V vs. Fc^+/Fc, only points outside of the saturation range were included in the linear fits.

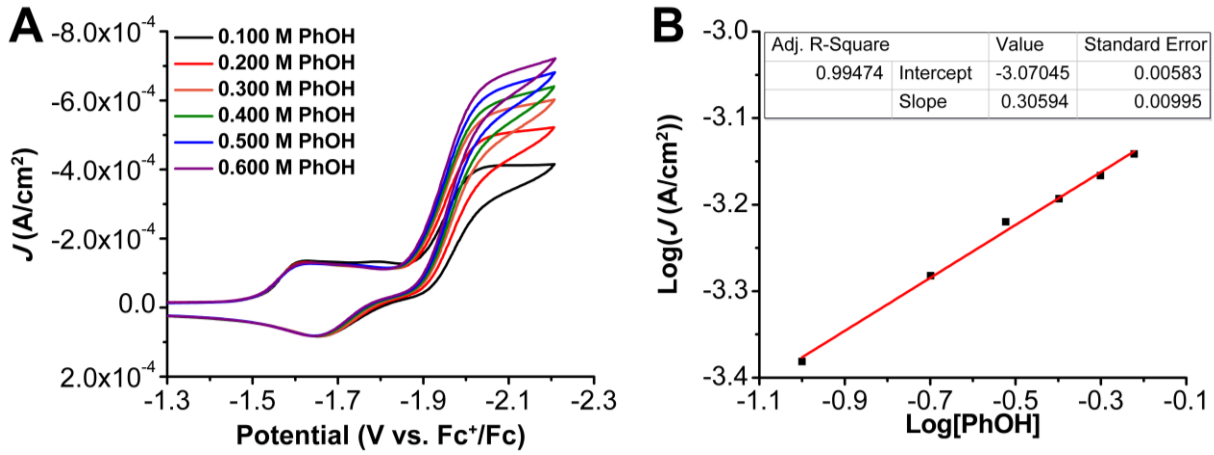

Figure S38. (A) CVs of 1.0 mM Cr(^{nPr}dhbpy)Cl(H_2O) **2**, obtained under CO_2 saturation conditions with variable PhOH concentration.Conditions: 1.0 mM **2**, 0.1 M $TBAPF_6$/DMF; glassy carbon disc working electrode, glassy carbon rod counter electrode, Ag/AgCl pseudoreference electrode; 100 mV/s scan rate; referenced to internal ferrocene standard. (**B**) Log-log plot from data obtained from CVs in **A** at −2.20 V vs. Fc^+/Fc.

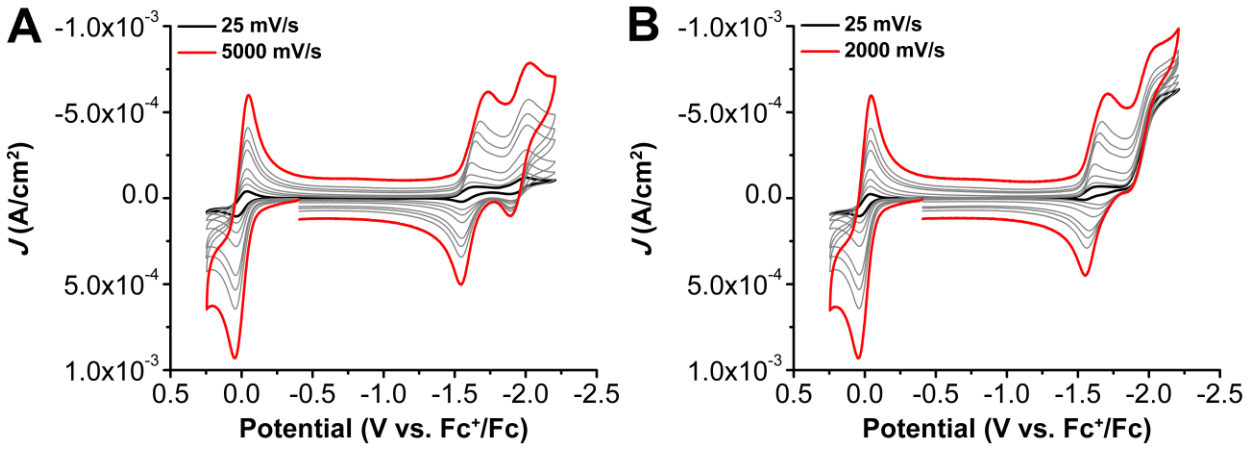

Figure S39. (**A**) CVs of Cr(^{nPr}dhbpy)Cl(H_2O) **2** with 0.6 M PhOH at variable scan rates ranging from 25 (black) to 2000 (red) mV/s, obtained under Ar (**A**) and CO_2 (**B**) saturation conditions. Conditions 1.0 mM **2**, 0.1 M $TBAPF_6$/DMF; glassy carbon working electrode, glassy carbon counter electrode, Ag/AgCl pseudoreference electrode; varied scan rate; referenced to internal ferrocene standard.

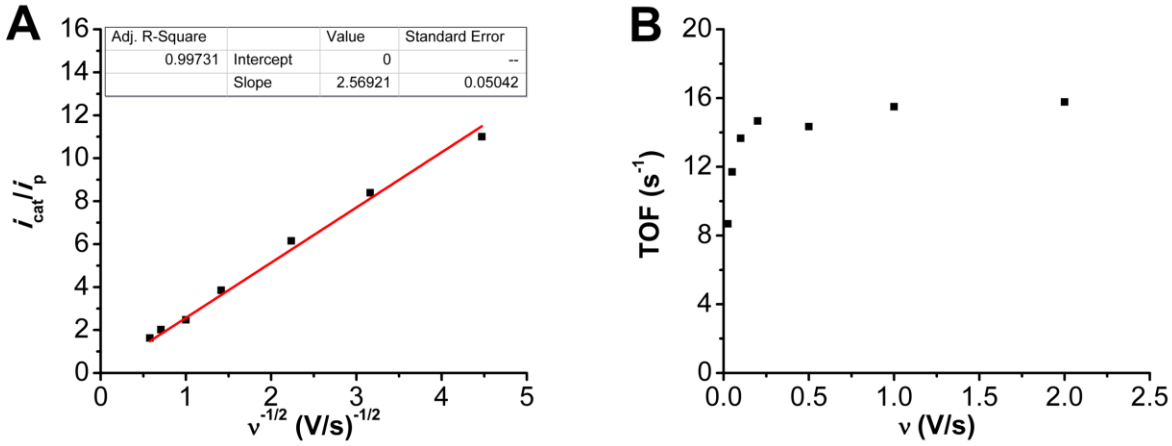

Figure S40. Plots of (**A**) i_{cat}/i_p versus the inverse of the square root of the scan rate and (**B**) TOF versus scan rate for 1.0 mM Cr(^{nPr}dhbpy)Cl(H_2O) **2**, with 0.6 M PhOH from data in Figure **S39**.

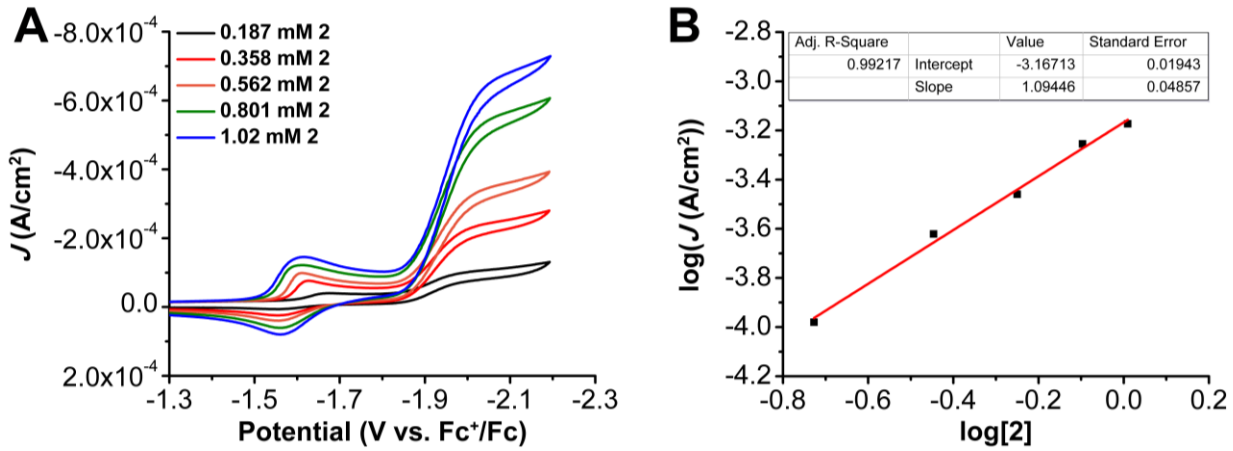

Figure S41. (**A**) CVs of Cr(^{nPr}dhbpy)Cl(H_2O) **2** at variable concentrations, obtained under CO_2 saturation with 1.0 M TFE. Conditions: 0.1 M $TBAPF_6$/DMF; glassy carbon disc working electrode, glassy carbon rod counter electrode, Ag/AgCl pseudoreference electrode; 100 mV/s scan rate; referenced to internal ferrocene standard. (**B**) Log-log plot from data obtained from CVs in **A** at −2.02 V vs. Fc^+/Fc.

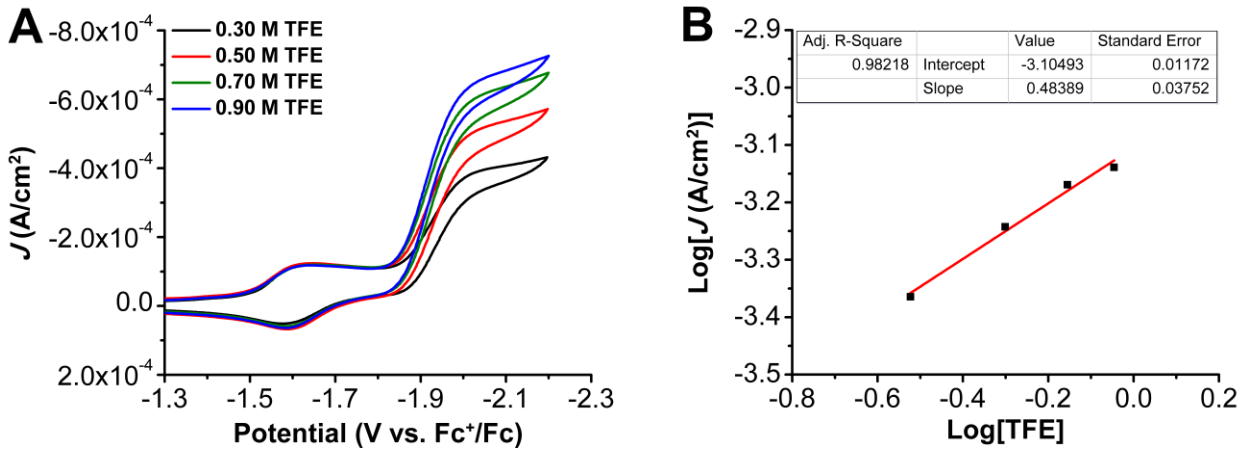

Figure S42. (**A**) CVs of 1.0 mM Cr(^{nPr}dhbpy)Cl(H_2O) **2** obtained under CO_2 concentration conditions with variable TFE concentration. Conditions: 1.0 mM **2**, 0.1 M $TBAPF_6$/DMF; glassy carbon disc working electrode, glassy carbon rod counter electrode, Ag/AgCl pseudoreference electrode; 100 mV/s scan rate; referenced to internal ferrocene standard. (**B**) Log–log plot from data obtained from CVs in **A** at −2.04 V vs. Fc^+/Fc, only points outside of the saturation range were included in the linear fits.

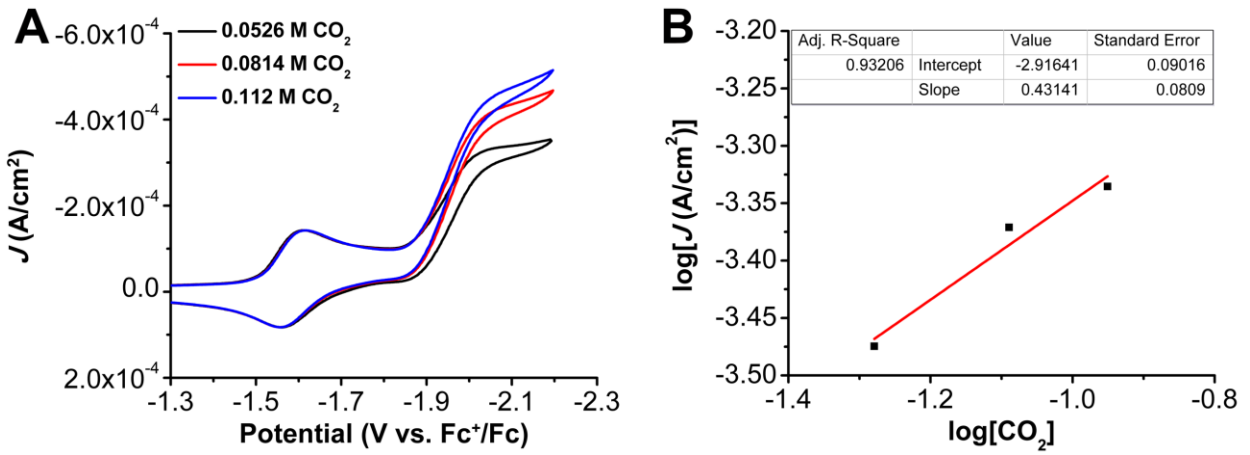

Figure S43. (**A**) CVs of 1.0 mM Cr(^{nPr}dhbpy)Cl(H_2O) **2** obtained under variable CO_2 concentration with 1.0 M TFE. Conditions: 0.1 M $TBAPF_6$/DMF; glassy carbon disc working electrode, glassy carbon rod counter electrode, Ag/AgCl pseudoreference electrode; 100 mV/s scan rate; referenced to internal ferrocene standard. (**B**) Log–log plot from data obtained from CVs in **A** at −2.07 V vs. Fc^+/Fc, only points outside of the saturation range were included in the linear fits.

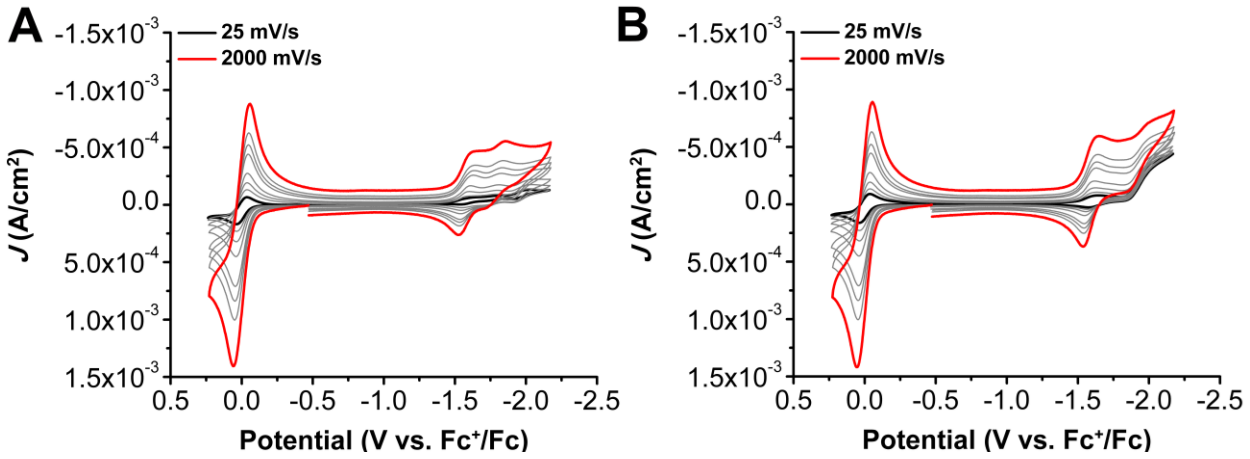

Figure S44. (**A**) CVs of Cr(^{nPr}dhbpy)Cl(H_2O) **2** with 1.0 M TFE at variable scan rates ranging from 25 (black) to 2000 (red) mV/s, obtained under Ar (**A**) and CO_2 (**B**) saturation conditions. Conditions 1.0 mM **2**, 0.1 M $TBAPF_6$/DMF; glassy carbon working electrode, glassy carbon counter electrode, Ag/AgCl pseudoreference electrode; varied scan rate; referenced to internal ferrocene standard.

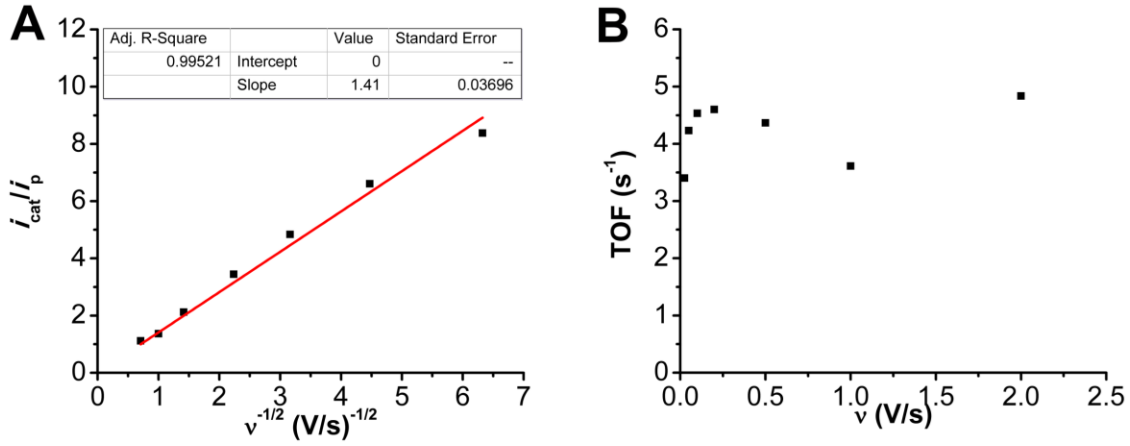

Figure S45. Plots of (**A**) i_{cat}/i_p versus the inverse of the square root of the scan rate and (**B**) TOF versus scan rate for 1.0 mM Cr(^{nPr}dhbpy)Cl(H_2O) **2**, with 1.0 M TFE from data in Figure **S44**.

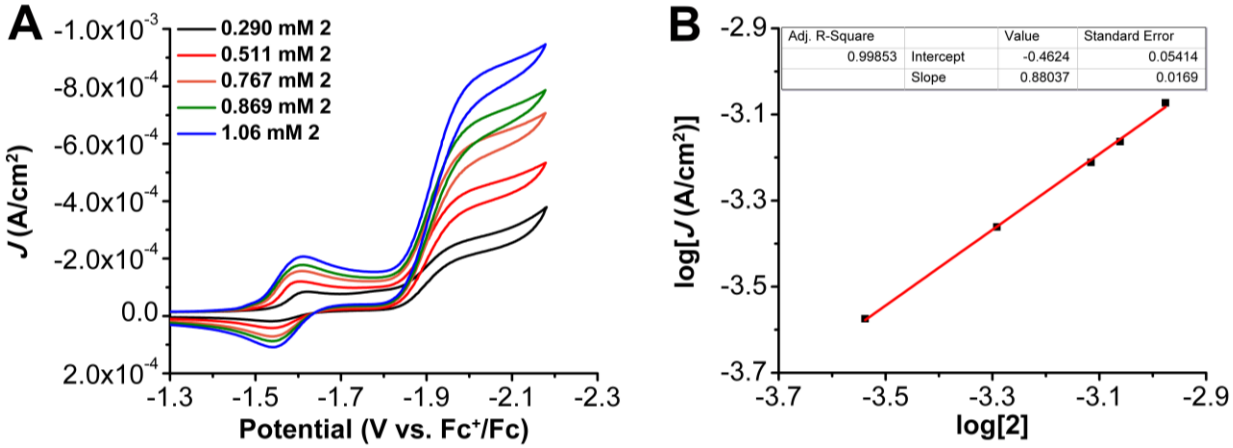

Figure S46. (**A**) CVs of Cr(^{nPr}dhbpy)Cl(H_2O) **2** at variable concentrations, obtained under CO_2 saturation with 20 mM TEAHPF_6. Conditions: 0.1 M TBAPF_6/DMF; glassy carbon disc working electrode, glassy carbon rod counter electrode, Ag/AgCl pseudoreference electrode; 100 mV/s scan rate; referenced to internal ferrocene standard. (**B**) Log-log plot from data obtained from CVs in **A** at −2.01 V vs. Fc^+/Fc.

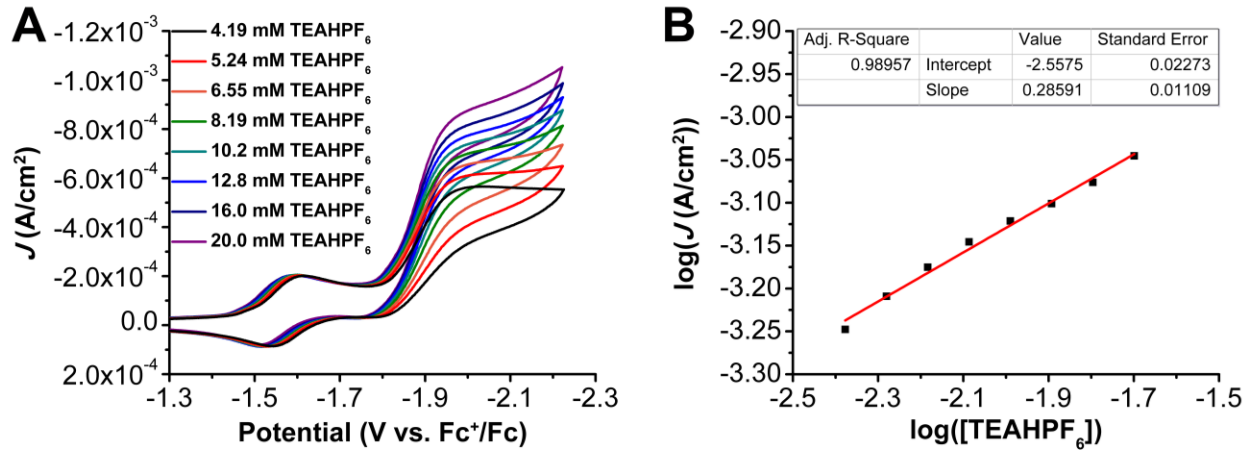

Figure S47. (**A**) CVs of 1.0 mM Cr(^{nPr}dhbpy)Cl(H_2O) **2**, obtained under CO_2 saturation conditions with variable $TEAHPF_6$ concentration.Conditions: 1.0 mM **2**, 0.1 M $TBAPF_6$/DMF; glassy carbon disc working electrode, glassy carbon rod counter electrode, Ag/AgCl pseudoreference electrode; 100 mV/s scan rate; referenced to internal ferrocene standard. (**B**) Log-log plot from data obtained from CVs in **A** at −2.02 V vs. Fc^+/Fc.

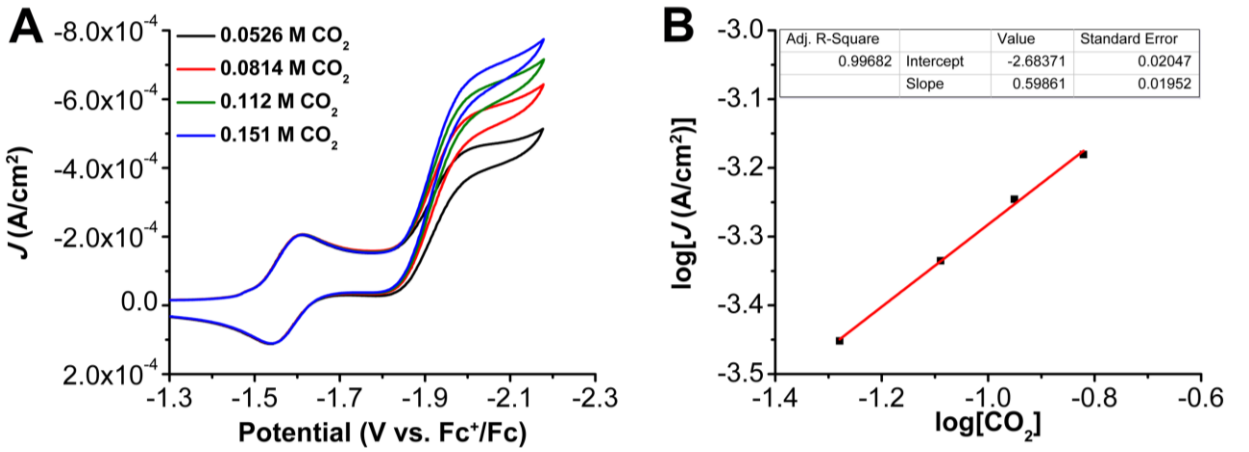

Figure S48. (A) CVs of 1.0 mM Cr(^{nPr}dhbpy)Cl(H_2O) **2** obtained under variable CO_2 concentration with 20 mM $TEAHPF_6$. Conditions: 0.1 M $TBAPF_6$/DMF; glassy carbon disc working electrode, glassy carbon rod counter electrode, Ag/AgCl pseudoreference electrode; 100 mV/s scan rate; referenced to internal ferrocene standard. (**B**) Log–log plot from data obtained from CVs in **A** at −2.02 V vs. Fc^+/Fc, only points outside of the saturation range were included in the linear fits.

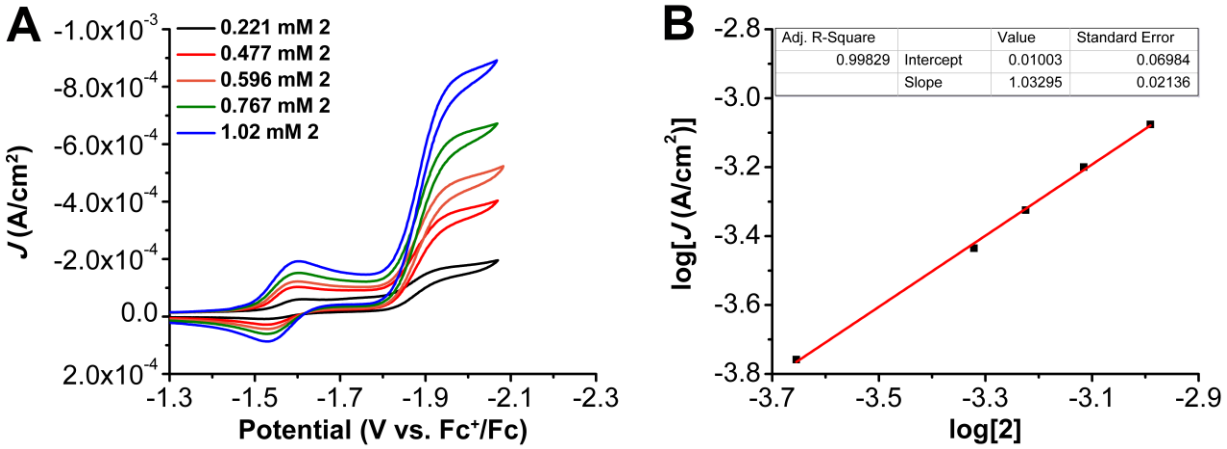

Figure S49. (**A**) CVs of Cr(^{nPr}dhbpy)Cl(H_2O) **2** at variable concentrations, obtained under CO_2 saturation with 0.1 M TEAHPF$_6$. Conditions: 0.1 M TBAPF$_6$/DMF; glassy carbon disc working electrode, glassy carbon rod counter electrode, Ag/AgCl pseudoreference electrode; 100 mV/s scan rate; referenced to internal ferrocene standard. (**B**) Log-log plot from data obtained from CVs in **A** at −1.98 V vs. Fc^+/Fc.

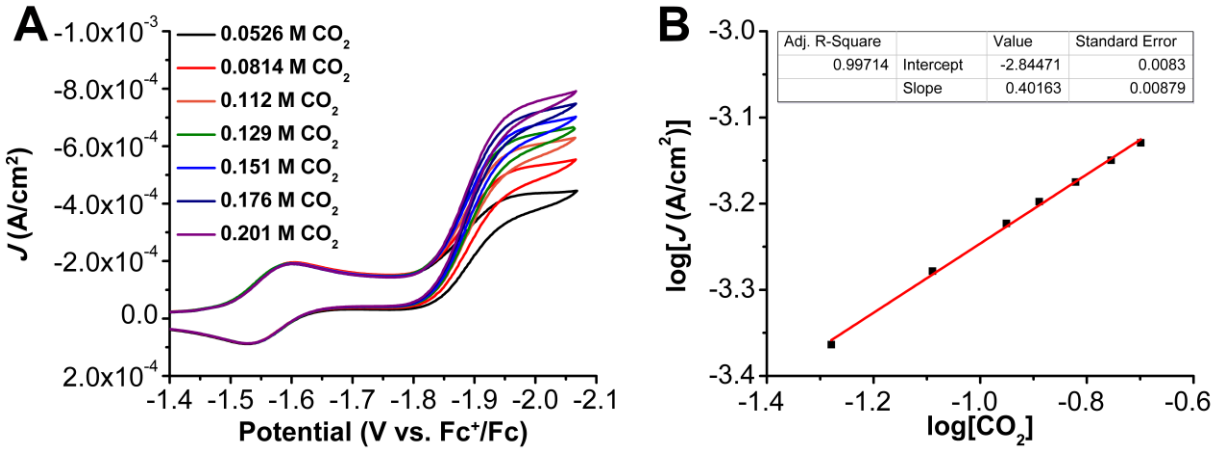

Figure S50. (A) CVs of 1.0 mM Cr(^{nPr}dhbpy)Cl(H_2O) **2** obtained under variable CO_2 concentration with 0.1 M TEAHPF$_6$. Conditions: 0.1 M TBAPF$_6$/DMF; glassy carbon disc working electrode, glassy carbon rod counter electrode, Ag/AgCl pseudoreference electrode; 100 mV/s scan rate; referenced to internal ferrocene standard. (**B**) Log–log plot from data obtained from CVs in **A** at −1.98 V vs. Fc^+/Fc, only points outside of the saturation range were included in the linear fits.

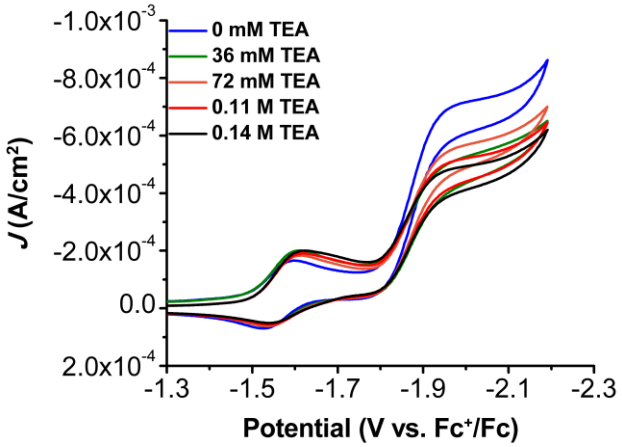

Figure S51. CVs of 1.0 mM Cr(^{nPr}dhbpy)Cl(H_2O) **2** and $TEAHPF_6$ obtained under CO_2 saturation with variable TEA. Conditions: 0.15 M $TEAHPF_6$ and 0.1 M $TBAPF_6$/DMF; glassy carbon disc working electrode, glassy carbon rod counter electrode, Ag/AgCl pseudoreference electrode; 100 mV/s scan rate; referenced to internal ferrocene standard.

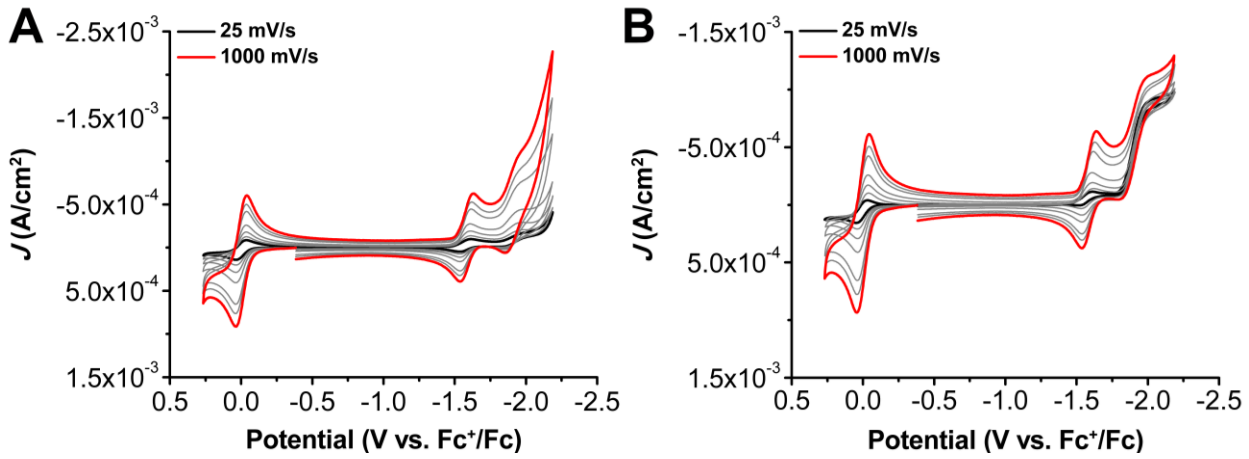

Figure S52. (**A**) CVs of Cr(^{nPr}dhbpy)Cl(H_2O) **2** with 20 mM $TEAHPF_6$ at variable scan rates ranging from 25 (black) to 1000 (red) mV/s, obtained under Ar (**A**) and CO_2 (**B**) saturation conditions. Conditions 1.0 mM **2**, 0.1 M $TBAPF_6$/DMF; glassy carbon working electrode, glassy carbon counter electrode, Ag/AgCl pseudoreference electrode; varied scan rate; referenced to internal ferrocene standard.

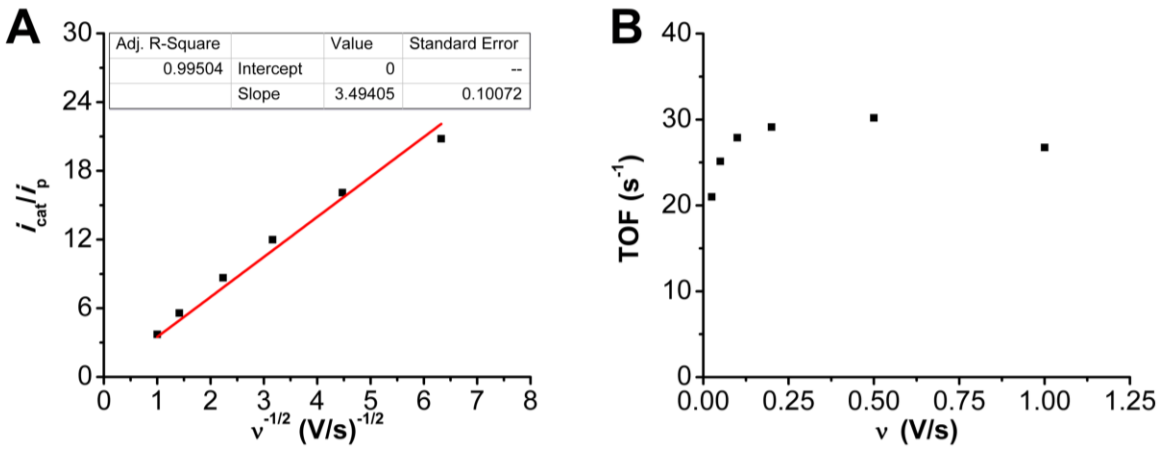

Figure S53. Plots of (**A**) i_{cat}/i_p versus the inverse of the square root of the scan rate and (**B**) TOF versus scan rate for 1.0 mM Cr(^{nPr}dhbpy)Cl(H_2O) **2**, with 20 mM TEAHPF$_6$ from data in Figure **S52**.

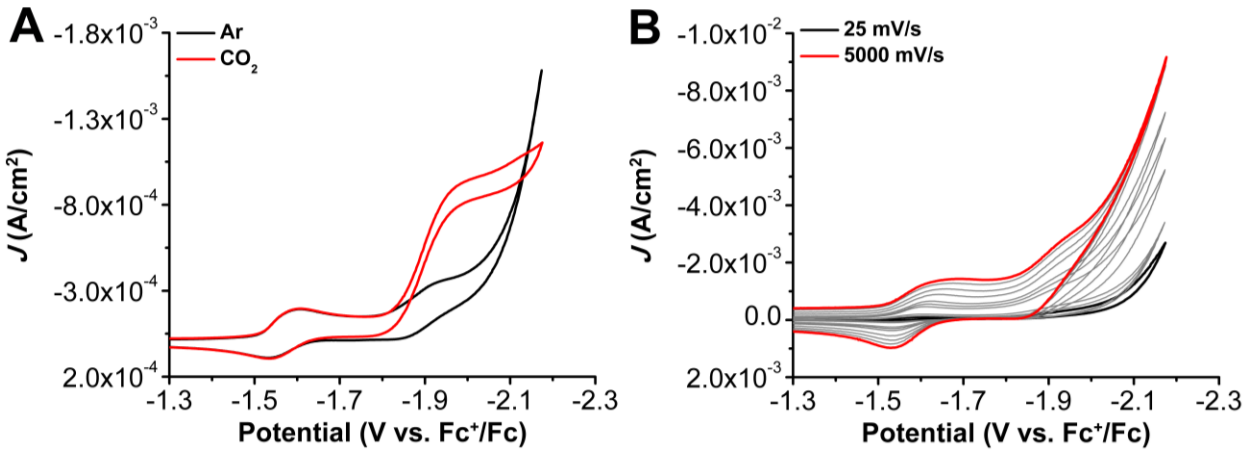

Figure S54. (**A**) CVs of 1.0 mM Cr(^{nPr}dhbpy)Cl(H_2O) **2** obtained under Ar and CO_2 saturation conditions. (**B**) CVs of 1.0 mM Cr(^{nPr}dhbpy)Cl(H_2O) **2** obtained under Ar saturation conditions at variable scan rates. Conditions: 1.0 mM **2** and 0.1 M TEAHPF$_6$/DMF; glassy carbon disc working electrode, glassy carbon rod counter electrode, Ag/AgCl pseudoreference electrode; 100 mV/s scan rate; referenced to internal ferrocene standard.

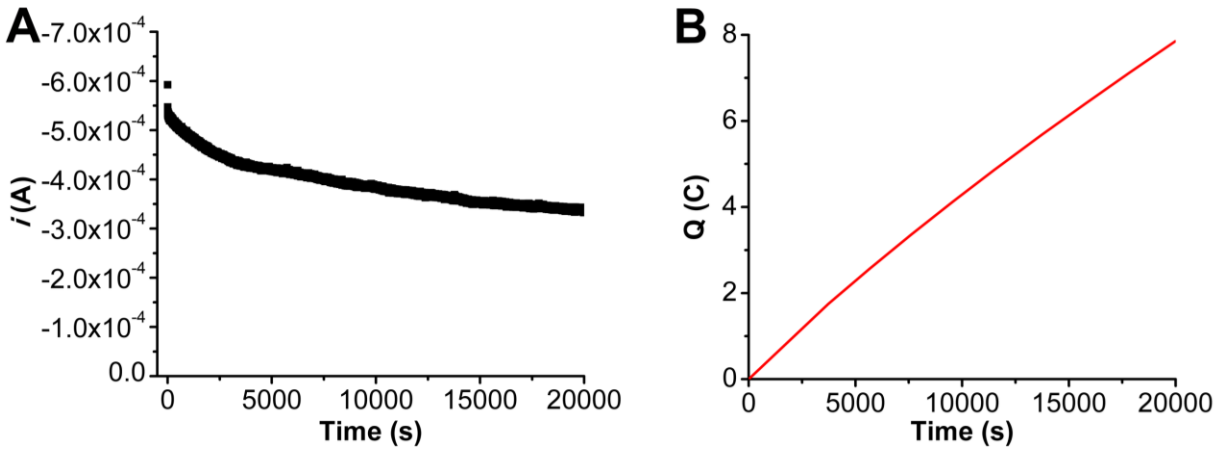

Figure S55. (**A**) Current versus time trace from CPE experiment for **2** + PhOH. (**B**) Charge passed versus time for the CPE experiment shown in **A**. Conditions were 0.5 mM Cr(^{nPr}dhbpy)Cl(H_2O) **2** and 1.0 M PhOH under a CO_2 atmosphere at −2.10 V vs Fc^+/Fc in 0.1 M $TBAPF_6$/DMF; working electrode was a glassy carbon rod, counter electrode was a graphite rod, and the reference was a nonaqueous Ag/AgCl pseudoreference electrode; 0.075 M Fc was used as sacrificial oxidant.

Table S10. Results from CPE experiment in **Figure S55**, 0.5 mM **2** + 1.0 M PhOH.

Time (s)	Charge (coulombs)	moles (e^-)	Moles of CO	FE_{CO}
19984*	7.85	8.14 x 10^{-5}	4.24 x 10^{-5}	104.24
19984*	7.85	8.14 x 10^{-5}	3.91 x 10^{-5}	96.16
19984*	7.85	8.14 x 10^{-5}	3.95 x 10^{-5}	97.15
19984*	7.85	8.15 x 10^{-5}	4.07 x 10^{-5}	99.94

* indicates a series of injections carried out upon completion of electrolysis.

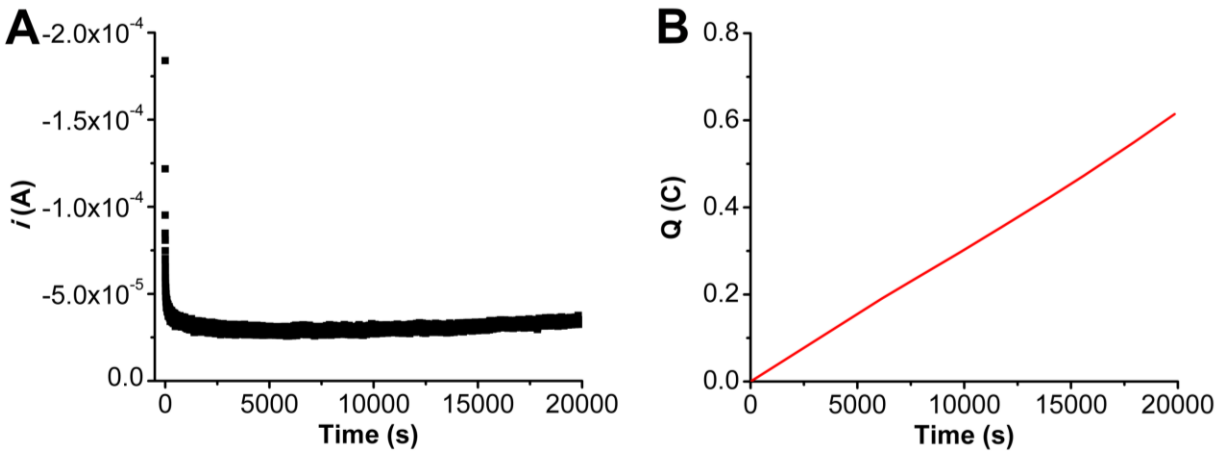

Figure S56. (**A**) Current versus time trace from rinse test of CPE experiment in **Figure S55** (**B**) Charge passed versus time for the CPE experiment shown in **A**. Conditions were 1.0 M PhOH under a CO_2 atmosphere at −2.1 V vs Fc^+/Fc in 0.1 M $TBAPF_6$/DMF; working electrode was the glassy carbon rod used in the experiment shown in **Figure S55** that was rinsed with DMF and not polished, counter electrode was a graphite rod, and the reference was a nonaqueous Ag/AgCl pseudoreference electrode; 0.075 M Fc was used as sacrificial oxidant.

Table S11. Results from CPE experiment in **Figure S56**.

Time (s)	Charge (coulombs)	moles (e^-)	Moles of CO	Moles of H_2
19847*	0.614	6.37×10^{-6}	<LOQ	<LOQ
19847*	0.614	6.37×10^{-6}	<LOQ	<LOQ
19847*	0.614	6.37×10^{-6}	<LOQ	<LOQ

* indicates a triplicate series of injections carried out upon completion of electrolysis.

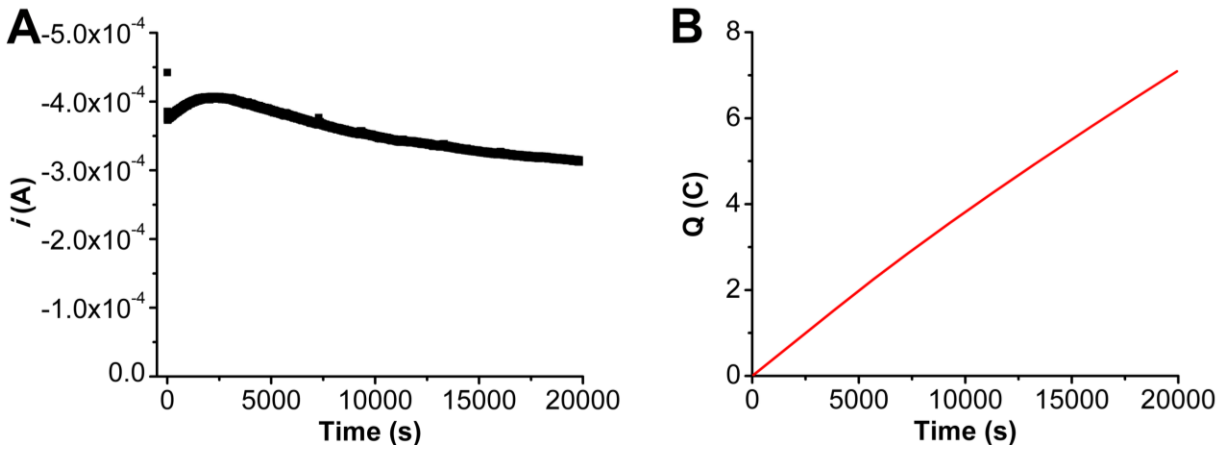

Figure S57. (**A**) Current versus time trace from CPE experiment for **2** + TFE. (**B**) Charge passed versus time for the CPE experiment shown in **A**. Conditions were 0.5 mM Cr(^{nPr}dhbpy)Cl(H_2O) **2** and 1.0 M TFE under a CO_2 atmosphere at −2.10 V vs Fc^+/Fc in 0.1 M $TBAPF_6$/DMF; working electrode was a glassy carbon rod, counter electrode was a graphite rod, and the reference was a nonaqueous Ag/AgCl pseudoreference electrode; 0.075 M Fc was used as sacrificial oxidant.

Table S12. Results from CPE experiment in **Figure S57**, 0.5 mM **2** + 1.0 M TFE.

Time (s)	Charge (coulombs)	moles (e^-)	Moles of CO	FE_{CO}
11920	4.26	4.42 x 10^{-5}	2.23 x 10^{-5}	100.8
13260	4.93	5.11 x 10^{-5}	2.68 x 10^{-5}	105.0
15945	5.82	6.03 x 10^{-5}	3.49 x 10^{-5}	115.7
17910	6.45	6.68 x 10^{-5}	3.98 x 10^{-5}	119.0
19937*	7.09	7.35 x 10^{-5}	4.41 x 10^{-5}	120.0
19937*	7.09	7.35 x 10^{-5}	3.44 x 10^{-5}	93.7
19937*	7.09	7.35 x 10^{-5}	3.37 x 10^{-5}	91.6
19937*	7.09	7.35 x 10^{-5}	3.33 x 10^{-5}	90.7

* indicates a series of injections carried out upon completion of electrolysis.

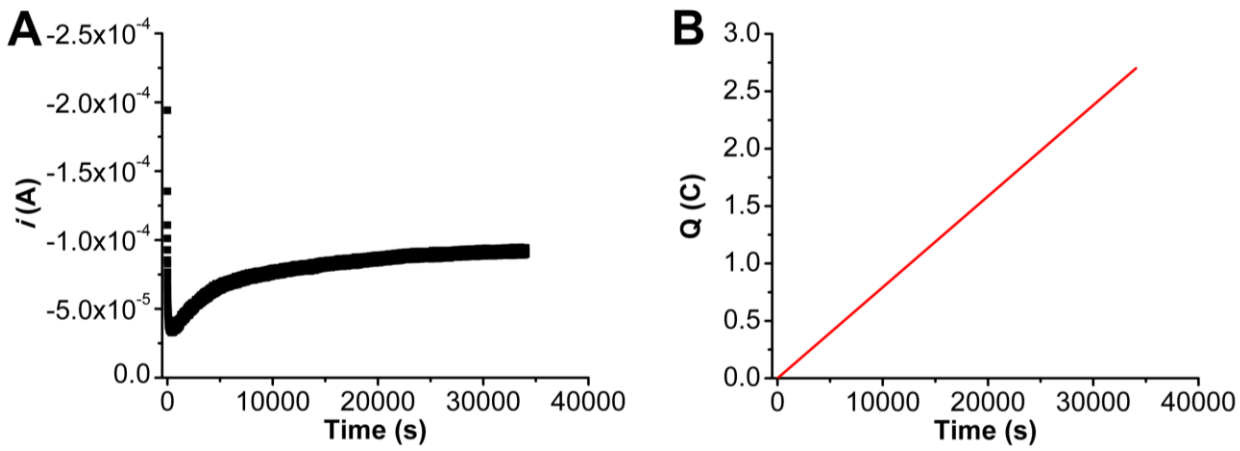

Figure S58. (**A**) Current versus time trace from rinse test of CPE experiment in **Figure S57** (**B**) Charge passed versus time for the CPE experiment shown in **A**. Conditions were 1.0 M TFE under a CO_2 atmosphere at −2.1 V vs Fc^+/Fc in 0.1 M $TBAPF_6$/DMF; working electrode was the glassy carbon rod used in the experiment shown in **Figure S57**that was rinsed with DMF and not polished, counter electrode was a graphite rod, and the reference was a nonaqueous Ag/AgCl pseudoreference electrode; 0.075 M Fc was used as sacrificial oxidant.

Table S13. Results from CPE experiment in **Figure S58**.

Time (s)	Charge (coulombs)	moles (e^-)	Moles of CO	Moles of H_2
34061*	2.70	2.80×10^{-5}	<LOQ	1.25×10^{-5}
34061*	2.70	2.80×10^{-5}	<LOQ	1.05×10^{-5}
34061*	2.70	2.80×10^{-5}	<LOQ	9.98×10^{-6}

* indicates a triplicate series of injections carried out upon completion of electrolysis.

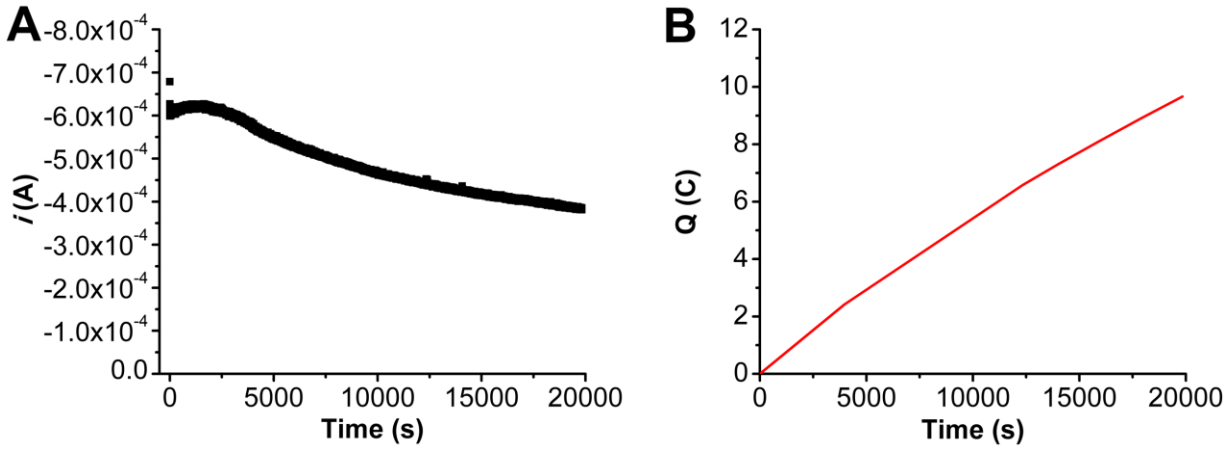

Figure S59. (**A**) Current versus time trace from CPE experiment for **2** + $TEAHPF_6$. (**B**) Charge passed versus time for the CPE experiment shown in **A**. Conditions were 0.4 mM Cr(^{nPr}dhbpy)Cl(H_2O) (**2**), 16 mM $TEAHPF_6$ under a CO_2 atmosphere at −2.1 V vs Fc^+/Fc in 0.1 M $TBAPF_6$/DMF; working electrode was a graphite rod, counter electrode was a graphite rod, and the reference was a nonaqueous Ag/AgCl pseudoreference electrode; 0.075 M Fc was used as sacrificial oxidant.

Table S14. Results from CPE experiment in **Figure S59**, 0.4 mM **2** + 16 mM $TEAHPF_6$.

Time (s)	Charge (coulombs)	moles (e^-)	Moles of CO	FE_{CO}	FE_{H2}
12335	6.58	6.82×10^{-5}	3.36×10^{-5}	98.62	<LOQ
13995	7.30	7.57×10^{-5}	3.85×10^{-5}	101.8	<LOQ
15890	8.02	8.39×10^{-5}	4.36×10^{-5}	103.9	<LOQ
17920	8.91	9.24×10^{-5}	4.78×10^{-5}	103.4	<LOQ
80156*	9.66	1.00×10^{-4}	5.07×10^{-5}	101.2	<LOQ
80156*	9.66	1.00×10^{-4}	5.55×10^{-5}	110.8	<LOQ
80156*	9.66	1.00×10^{-4}	5.53×10^{-5}	110.5	<LOQ

* indicates a triplicate series of injections carried out upon completion of electrolysis

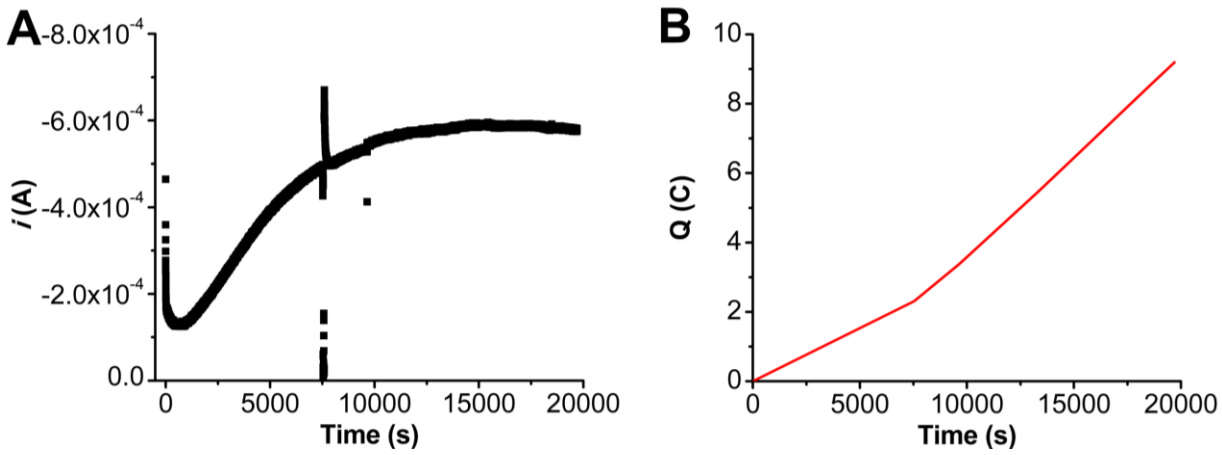

Figure S60. (**A**) Current versus time trace from rinse test of CPE experiment in **Figure S59** (**B**) Charge passed versus time for the CPE experiment shown in A. Conditions were 20 mM $TEAHPF_6$ under a CO_2 atmosphere at −2.1 V vs Fc^+/Fc in 0.1 M $TBAPF_6$/DMF; working electrode was the glassy carbon rod used in the experiment shown in **Figure S59**that was rinsed with DMF and not polished, counter electrode was a graphite rod, and the reference was a nonaqueous Ag/AgCl pseudoreference electrode; 0.075 M Fc was used as sacrificial oxidant.

Table S15. Results from CPE experiment in **Figure S60**.

Time (s)	Charge (coulombs)	moles (e^-)	Moles of CO	Moles of H_2
13340	5.47	5.67×10^{-5}	<LOQ	2.01×10^{-5}
15420	6.69	6.93×10^{-5}	<LOQ	2.50×10^{-5}
18480	8.49	8.80×10^{-5}	<LOQ	3.07×10^{-5}
19700*	9.20	9.53×10^{-5}	<LOQ	3.43×10^{-5}
19700*	9.20	9.53×10^{-5}	<LOQ	3.14×10^{-5}
19700*	9.20	9.53×10^{-5}	<LOQ	3.04×10^{-5}

* indicates a triplicate series of injections carried out upon completion of electrolysis.

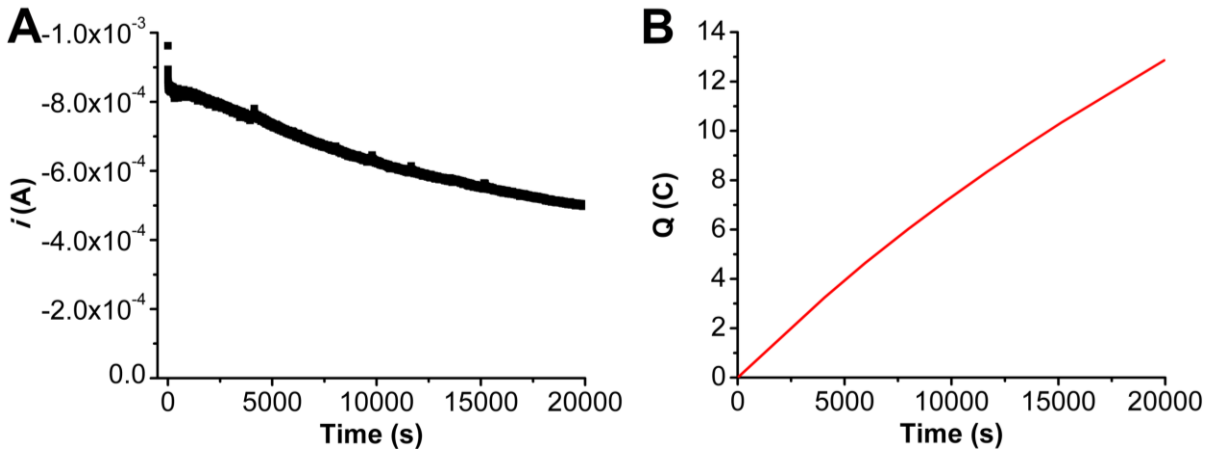

Figure S61. (**A**) Current versus time trace from CPE experiment for **2** + $TEAHPF_6$. (**B**) Charge passed versus time for the CPE experiment shown in (**A**). Conditions were 0.5 mM Cr(^{nPr}-bpy)Cl(H_2O) (**2**), 0.1 M $TEAHPF_6$ in DMF under a CO_2 atmosphere at −2.05 V vs Fc^+/Fc; working electrode was a graphite rod, counter electrode was a graphite rod, and the reference was a nonaqueous Ag/AgCl pseudoreference electrode; 0.075 M Fc was used as sacrificial oxidant.

Table S16. Results from CPE experiment in **Figure S61**, 0.5 mM **2** + 0.1 M $TEAHPF_6$.

Time (s)	Charge (coulombs)	moles (e^-)	Moles of CO	FE_{CO}	FE_{H2}
13535	9.43	9.78×10^{-5}	4.59×10^{-5}	93.95	<LOQ
15150	10.34	1.07×10^{-4}	5.44×10^{-5}	101.5	<LOQ
19953*	12.86	1.33×10^{-4}	7.21×10^{-5}	108.1	<LOQ
19953*	12.86	1.33×10^{-4}	6.97×10^{-5}	104.5	<LOQ
19953*	12.86	1.33×10^{-4}	7.19×10^{-5}	107.80	<LOQ
19953*	12.86	1.33×10^{-4}	7.00×10^{-5}	105.0	<LOQ

* indicates a series of injections carried out upon completion of electrolysis

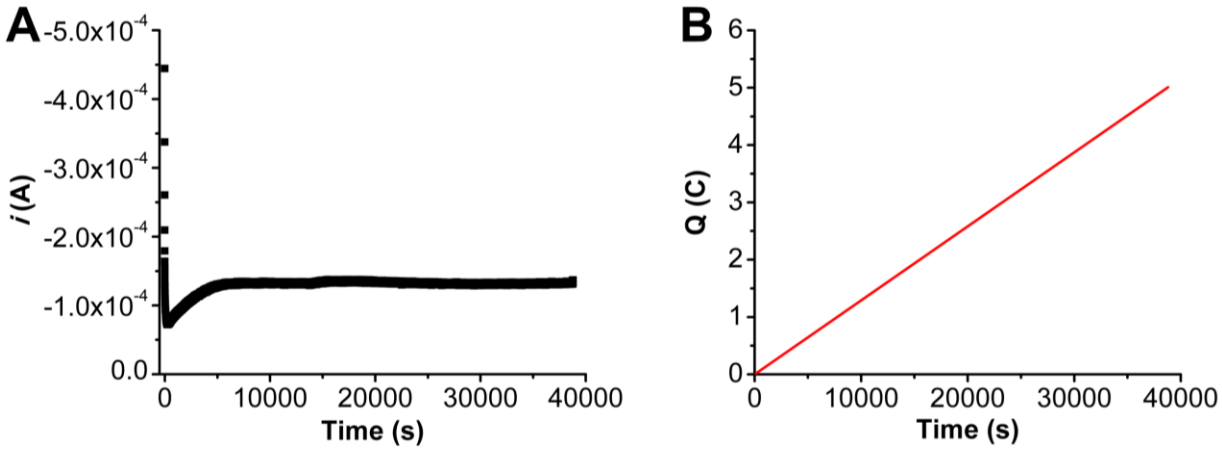

Figure S62. (**A**) Current versus time trace from rinse test of CPE experiment in **Figure S61** (**B**) Charge passed versus time for the CPE experiment shown in **A**. Conditions were 20 mM $TEAHPF_6$ under a CO_2 atmosphere at −2.05 V vs Fc^+/Fc in DMF; working electrode was the glassy carbon rod used in the experiment shown in **Figure S61** that was rinsed with DMF and not polished, counter electrode was a graphite rod, and the reference was a nonaqueous Ag/AgCl pseudoreference electrode; 0.075 M Fc was used as sacrificial oxidant.

Table S17. Results from CPE experiment in **Figure S62**.

Time (s)	Charge (coulombs)	moles (e^-)	Moles of CO	Moles of H_2
38803*	5.01	5.19×10^{-5}	<LOQ	1.66×10^{-5}
38803*	5.01	5.19×10^{-5}	<LOQ	1.56×10^{-5}
38803*	5.01	5.19×10^{-5}	<LOQ	1.55×10^{-5}
38803*	5.01	5.19×10^{-5}	<LOQ	1.54×10^{-5}

* indicates a series of injections carried out upon completion of electrolysis.

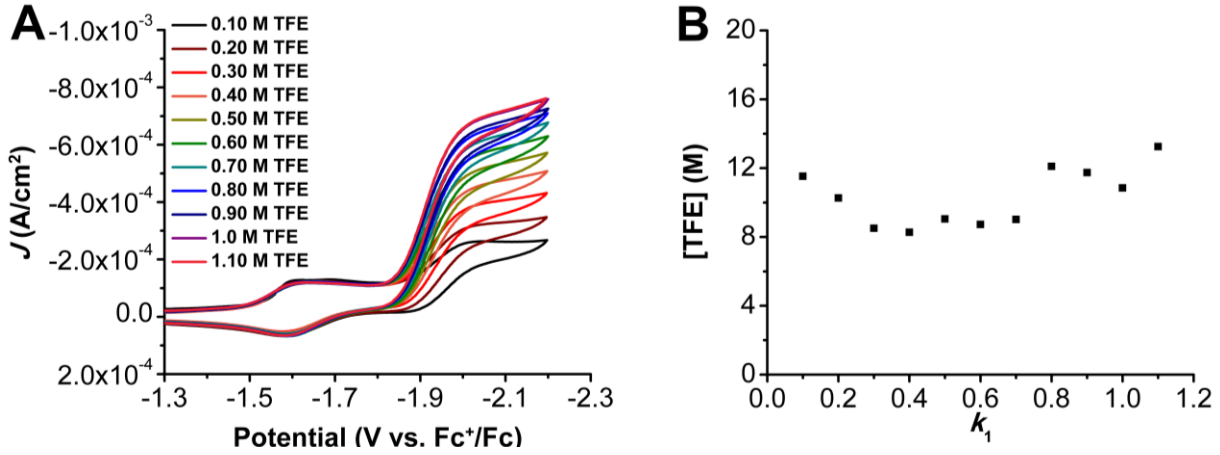

Figure S63. (**A**) CVs of 1.0 mM Cr(^{nPr}dhbpy)Cl(H_2O) **2** obtained under CO_2 saturation with variable concentrations of TFE. Conditions: 0.1 M $TBAPF_6$/DMF; glassy carbon disc working electrode, glassy carbon rod counter electrode, Ag/AgCl pseudoreference electrode; 100 mV/s scan rate; referenced to internal ferrocene standard. (**B**) Plot of k_1 versus [TFE] from data obtained from shifts in $E_{cat/2}$ from (**A**) using **Eq (S5)** as described above.

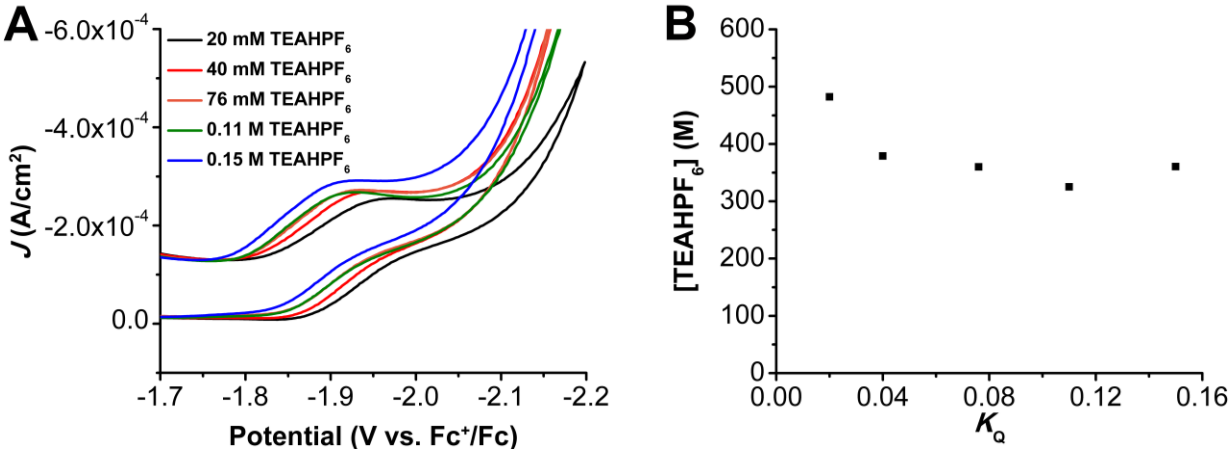

Figure S64. (**A**) CVs of 1.0 mM Cr(^{nPr}dhbpy)Cl(H_2O) **2** obtained under Ar saturation with variable concentrations of $TEAHPF_6$. Conditions: 0.1 M $TBAPF_6$/DMF; glassy carbon disc working electrode, glassy carbon rod counter electrode, Ag/AgCl pseudoreference electrode; 100 mV/s scan rate; referenced to internal ferrocene standard. (**B**) Plot of K_Q versus [$TEAHPF_6$] from data obtained from shifts in E from **A** and using **Eq. (S6)** to determine K_Q as described above.

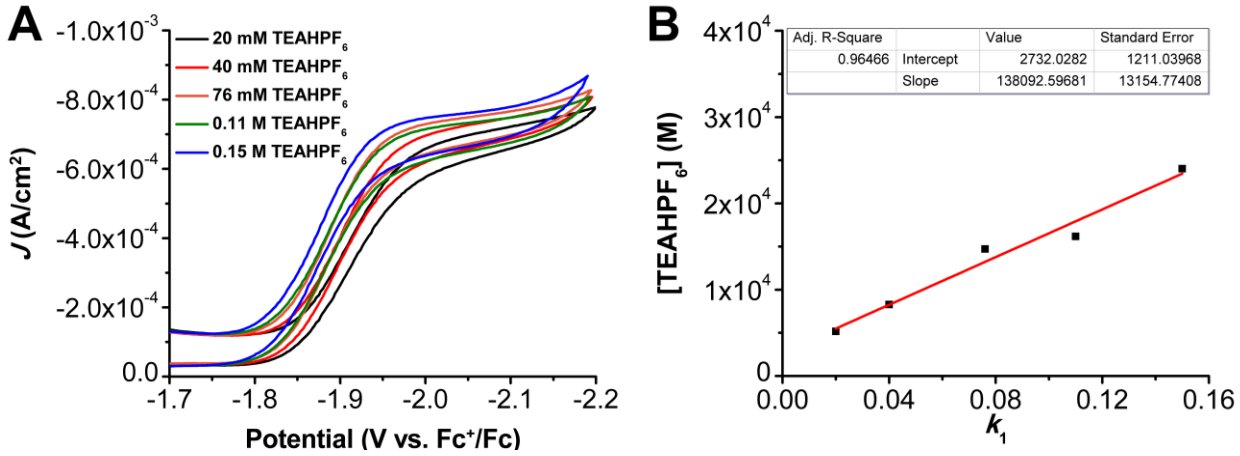

Figure S65. (**A**) CVs of 1.0 mM Cr(^{nPr}dhbpy)Cl(H_2O) **2** obtained under CO_2 saturation with variable concentrations of $TEAHPF_6$. Conditions: 0.1 M $TBAPF_6$/DMF; glassy carbon disc working electrode, glassy carbon rod counter electrode, Ag/AgCl pseudoreference electrode; 100 mV/s scan rate; referenced to internal ferrocene standard. (**B**) Plot of k_1 versus [$TEAHPF_6$] from data obtained from shifts in $E_{cat/2}$ from (**A**) using **Eq (S5)** as described above.

Computational Methods

Geometry optimizations were performed without geometry constraints at the DFT level with the Gaussian 16 program, Rev B.01,[26] employing the hybrid functional B3LYP[27-30] and the def2-SVP basis set was used for all atoms.[31, 32] Dispersion and bulk solvent effects (*N*,*N*-dimethylformamide = DMF; ε = 37.219) were accounted for at the optimization stage, by using Grimme's D3 parameter set with Becke-Johnson (BJ) damping[33, 34] and the CPCM continuum model,[35] respectively. The stationary points and their nature as minima (no imaginary frequencies) were characterized by vibrational analysis using the IGRRHO approach as implemented by default in the software package, which also produced enthalpy (H), entropy (S) and Gibbs energy (G) data at 298.15 K. The minima connected by a given transition state were determined by perturbing the transition states along the TS coordinate and optimizing to the nearest minimum. Free energies were corrected (ΔG_{qh}) to account for concentration effects and for errors associated with the harmonic oscillator approximation. Thus, according to Truhlars's quasi-harmonic approximation for vibrational entropy and enthalpy, all vibrational frequencies below 100 cm^{-1} were set to this value.[36] These anharmonic and concentration corrections were calculated with the Goodvibes code.[37] Concentrations were set at 0.001 M for all molecules unless otherwise specified: 0.050 M for $TEAH^+$, 0.23 M for CO_2, and 12.92 M for DMF. Energies were refined by means of single point calculations with the larger def2-TZVP basis set. The stability of the wavefunction and spin contamination were studied at the double- and triple-zeta levels of theory.

References:

1. Hooe, S. L.; Dressel, J. M.; Dickie, D. A.; Machan, C. W. Highly Efficient Electrocatalytic Reduction of CO_2 to CO by a Molecular Chromium Complex. *ACS Catal.* **2020**, *10* (2), 1146-1151. DOI: 10.1021/acscatal.9b04687.
2. Pegis, M. L.; Wise, C. F.; Martin, D. J.; Mayer, J. M. Oxygen Reduction by Homogeneous Molecular Catalysts and Electrocatalysts. *Chem. Rev.* **2018**, *118* (5), 2340-2391. DOI: 10.1021/acs.chemrev.7b00542.
3. Hooe, S. L.; Dressel, J. M.; Dickie, D. A.; Machan, C. W. Highly Efficient Electrocatalytic Reduction of CO_2 to CO by a Molecular Chromium Complex. *ACS Catal.* **2020**, *10* (2), 1146-1151. DOI: 10.1021/acscatal.9b04687.
4. Izutsu, K. *Electrochemistry in Nonaqueous Solutions*; Wiley-VCH, 2009.
5. Hooe, S. L.; Rheingold, A. L.; Machan, C. W. Electrocatalytic Reduction of Dioxygen to Hydrogen Peroxide by a Molecular Manganese Complex with a Bipyridine-Containing Schiff Base Ligand. *J. Am. Chem. Soc.* **2018**, *140* (9), 3232-3241. DOI: 10.1021/jacs.7b09027.
6. Kütt, A.; Tshepelevitsh, S.; Saame, J.; Lõkov, M.; Kaljurand, I.; Selberg, S.; Leito, I. Strengths of Acids in Acetonitrile. *EurJOC* **2021**, *2021* (9), 1407-1419, https://doi.org/10.1002/ejoc.202001649. DOI: https://doi.org/10.1002/ejoc.202001649 (acccessed 2023/01/18).
7. Lam, Y. C.; Nielsen, R. J.; Gray, H. B.; Goddard, W. A., III. A Mn Bipyrimidine Catalyst Predicted To Reduce CO_2 at Lower Overpotential. *ACS Cat.* **2015**, *5* (4), 2521-2528. DOI: 10.1021/cs501963v.
8. Nielsen, M. F.; Hammerich, O.; Rise, F.; Gogoll, A.; Undheim, K.; Wang, D. N.; Christensen, S. B. The Effect of Hydrogen Bonding between Methyl-Substituted Phenols and Dipolar Aprotic Solvents on the Rate Constants for. *Acta. Chem. Scan.* **1992**, *46*, 883-896.
9. McCarthy, B. D.; Martin, D. J.; Rountree, E. S.; Ullman, A. C.; Dempsey, J. L. Electrochemical Reduction of Brønsted Acids by Glassy Carbon in Acetonitrile—Implications for Electrocatalytic Hydrogen Evolution. *Inorg. Chem.* **2014**, *53* (16), 8350-8361. DOI: 10.1021/ic500770k.
10. Roy, S.; Sharma, B.; Pécaut, J.; Simon, P.; Fontecave, M.; Tran, P. D.; Derat, E.; Artero, V. Molecular Cobalt Complexes with Pendant Amines for Selective Electrocatalytic Reduction of Carbon Dioxide to Formic Acid. *J. Am. Chem. Soc.* **2017**, *139* (10), 3685-3696. DOI: 10.1021/jacs.6b11474.
11. Matsubara, Y. Unified Benchmarking of Electrocatalysts in Noninnocent Second Coordination Spheres for CO2 Reduction. *ACS Energy Lett.* **2019**, *4* (8), 1999-2004. DOI: 10.1021/acsenergylett.9b01180.
12. Costentin, C.; Drouet, S.; Robert, M.; Savéant, J.-M. Turnover Numbers, Turnover Frequencies, and Overpotential in Molecular Catalysis of Electrochemical Reactions. Cyclic Voltammetry and Preparative-Scale Electrolysis. *J. Am. Chem. Soc.* **2012**, *134* (27), 11235-11242. DOI: 10.1021/ja303560c.
13. Costentin, C.; Drouet, S.; Robert, M.; Savéant, J.-M. Correction to Turnover Numbers, Turnover Frequencies, and Overpotential in Molecular Catalysis of Electrochemical Reactions. Cyclic Voltammetry and Preparative-Scale Electrolysis. *J. Am. Chem. Soc.* **2012**, *134* (48), 19949-19950. DOI: 10.1021/ja3106187.

14. Cometto, C.; Chen, L.; Lo, P.-K.; Guo, Z.; Lau, K.-C.; Anxolabéhère-Mallart, E.; Fave, C.; Lau, T.-C.; Robert, M. Highly Selective Molecular Catalysts for the CO2-to-CO Electrochemical Conversion at Very Low Overpotential. Contrasting Fe vs Co Quaterpyridine Complexes upon Mechanistic Studies. *ACS Catal.* **2018**, *8* (4), 3411-3417. DOI: 10.1021/acscatal.7b04412.
15. Reid, A. G.; Moreno, J. J.; Hooe, S. L.; Baugh, K. R.; Thomas, I. H.; Dickie, D. A.; Machan, C. W. Inverse potential scaling in co-electrocatalytic activity for CO_2 reduction through redox mediator tuning and catalyst design. *Chem. Sci.* **2022**, *13* (33), 9595-9606, 10.1039/D2SC03258A. DOI: 10.1039/D2SC03258A.
16. Baur, J. E. Chapter 19 Diffusion Coefficients. In *Handbook of Electrochemistry*, Zoski, C. G. Ed.; Elsevier, 2007; pp 829-848.
17. Costentin, C.; Saveant, J.-M. *Elements of Molecular and Biomolecular Electrochemistry: An Electrochemical Approach to Electron Transfer Chemistry*; John Wiley & Sons Inc., 2019. DOI: 10.1002/9781119292364.
18. Dressel, J. M.; Cook, E. N.; Hooe, S. L.; Moreno, J. J.; Dickie, D. A.; Machan, C. W. Electrocatalytic hydrogen evolution reaction by a Ni(N_2O_2) complex based on 2,2′-bipyridine. *Inorg. Chem. Front.* **2023**, *10* (3), 972-978, 10.1039/D2QI01928K. DOI: 10.1039/D2QI01928K.
19. *Saint; SADABS; APEX5*; Bruker AXS Inc. : Madison, Wisconsin, USA, 2012.
20. Krause, L.; Herbst-Irmer, R.; Sheldrick, G. M.; Stalke, D. Comparison of silver and molybdenum microfocus X-ray sources for single-crystal structure determination. *J. Appl. Cryst.* **2015**, *48* (1), 3-10. DOI: doi:10.1107/S1600576714022985.
21. Dolomanov, O. V.; Bourhis, L. J.; Gildea, R. J.; Howard, J. A. K.; Puschmann, H. OLEX2: a complete structure solution, refinement and analysis program. *J. Appl. Cryst.* **2009**, *42* (2), 339-341. DOI: doi:10.1107/S0021889808042726.
22. Nichols, A. W.; Cook, E. N.; Gan, Y. J.; Miedaner, P. R.; Dressel, J. M.; Dickie, D. A.; Shafaat, H. S.; Machan, C. W. Pendent Relay Enhances H_2O_2 Selectivity during Dioxygen Reduction Mediated by Bipyridine-Based Co–N_2O_2 Complexes. *J. Am. Chem. Soc.* **2021**, *143* (33), 13065-13073. DOI: 10.1021/jacs.1c03381.
23. Grant, D. H. Paramagnetic Susceptibility by NMR: The "Solvent Correction" Reexamined. *J. Chem. Educ.* **1995**, *72* (1), 39. DOI: 10.1021/ed072p39.
24. Bain, G. A.; Berry, J. F. Diamagnetic corrections and Pascal's constants. *J. Chem. Educ.* **2008**, *85* (4), 532-536, 10.1021/ed085p532. DOI: 10.1021/ed085p532.
25. Sathrum, A. J.; Kubiak, C. P. Kinetics and Limiting Current Densities of Homogeneous and Heterogeneous Electrocatalysts. *J. Phys. Chem. Lett.* **2011**, *2* (18), 2372-2379. DOI: 10.1021/jz2008227.
26. *Gaussian 16 Rev. B.01*; Wallingford, CT, 2016.
27. Becke, A. D. Density-functional thermochemistry. III. The role of exact exchange. *J. Chem. Phys.* **1993**, *98* (7), 5648-5652. DOI: doi:http://dx.doi.org/10.1063/1.464913.
28. Lee, C.; Yang, W.; Parr, R. G. Development of the Colle-Salvetti correlation-energy formula into a functional of the electron density. *Phys. Rev. B* **1988**, *37* (2), 785-789.
29. Vosko, S. H.; Wilk, L.; Nusair, M. Accurate spin-dependent electron liquid correlation energies for local spin density calculations: a critical analysis. *Can. J. Phys.* **1980**, *58* (8), 1200-1211. DOI: 10.1139/p80-159.

30. Stephens, P. J.; Devlin, F. J.; Chabalowski, C. F.; Frisch, M. J. Ab Initio Calculation of Vibrational Absorption and Circular Dichroism Spectra Using Density Functional Force Fields. *J. Phys. Chem.* **1994**, *98* (45), 11623-11627. DOI: 10.1021/j100096a001.
31. Weigend, F.; Ahlrichs, R. Balanced basis sets of split valence, triple zeta valence and quadruple zeta valence quality for H to Rn: Design and assessment of accuracy. *Phys. Chem. Chem. Phys.* **2005**, *7* (18), 3297-3305, 10.1039/B508541A. DOI: 10.1039/B508541A.
32. Weigend, F. Accurate Coulomb-fitting basis sets for H to Rn. *Phys. Chem. Chem. Phys.* **2006**, *8* (9), 1057-1065, 10.1039/B515623H. DOI: 10.1039/B515623H.
33. Grimme, S.; Antony, J.; Ehrlich, S.; Krieg, H. A consistent and accurate ab initio parametrization of density functional dispersion correction (DFT-D) for the 94 elements H-Pu. *J. Chem. Phys.* **2010**, *132* (15), 154104. DOI: doi:http://dx.doi.org/10.1063/1.3382344.
34. Grimme, S.; Ehrlich, S.; Goerigk, L. Effect of the damping function in dispersion corrected density functional theory. *J. Comput. Chem.* **2011**, *32* (7), 1456-1465. DOI: 10.1002/jcc.21759.
35. Barone, V.; Cossi, M. Quantum Calculation of Molecular Energies and Energy Gradients in Solution by a Conductor Solvent Model. *J. Phys. Chem. A* **1998**, *102* (11), 1995-2001. DOI: 10.1021/jp9716997.
36. Ribeiro, R. F.; Marenich, A. V.; Cramer, C. J.; Truhlar, D. G. Use of Solution-Phase Vibrational Frequencies in Continuum Models for the Free Energy of Solvation. *J. Phys. Chem. B* **2011**, *115* (49), 14556-14562. DOI: 10.1021/jp205508z.
37. *Goodvibes v3.0.1*; 2019. https://doi.org/10.5281/zenodo.3346166.